

BSC

## Design Calculation or Analysis Cover Sheet

Complete only applicable items.

1. QA: QA

2. Page 1

3. System Naval Waste Package	4. Document Identifier 000-00C-DN00-00300-000-00A
5. Title Naval Waste Package Design Sensitivity	
6. Group Thermal/Structural Analysis	
7. Document Status Designation <input type="checkbox"/> Preliminary <input checked="" type="checkbox"/> Committed <input type="checkbox"/> Confirmed <input type="checkbox"/> Cancelled/Superseded	

## 8. Notes/Comments

The calculations contained in this document were developed by Bechtel SAIC Company, LLC (BSC) and are intended solely for the use of BSC in its work for the Yucca Mountain Project.

The Thermal/Structural Analysis group has performed a sensitivity analysis in this calculation in response to Action Item 6335-001 of CR Number 6335.

Attachments		Total Number of Pages
See Section 5		

RECORD OF REVISIONS						
9. No.	10. Reason For Revision	11. Total # of Pgs.	12. Last Pg. #	13. Originator (Print/Sign/Date)	14. Checker (Print/Sign/Date)	15. Approved/Accepted (Print/Sign/Date)
00A	Initial Issue.	44	44	Tim Schmitt <i>FCB</i> <i>10/26/06</i>	Kenneth Jaquay <i>KJ</i> <i>10/26/06</i>	Michael J. Anderson <i>MJA</i> <i>10/26/06</i>

## CONTENTS

	Page
1. PURPOSE .....	5
2. REFERENCES.....	6
2.1 DESIGN INPUTS .....	6
2.2 DESIGN CONSTRAINTS .....	8
2.3 DESIGN OUTPUTS.....	9
3. ASSUMPTIONS .....	10
3.1 ASSUMPTIONS THAT REQUIRE VERIFICATION .....	10
3.2 ASSUMPTIONS THAT DO NOT REQUIRE VERIFICATION .....	10
4. METHODOLOGY .....	16
4.1 QUALITY ASSURANCE.....	16
4.2 USE OF SOFTWARE .....	16
4.3 STRESS ANALYSIS APPROACH .....	16
5. ATTACHMENTS .....	17
6. CALCULATION .....	19
6.1 USE OF COMPUTER SOFTWARE.....	19
6.2 MATERIAL PROPERTIES.....	20
6.2.1 Calculations for Elevated-Temperature Elongations .....	23
6.2.2 Calculations for True Measures of Ductility.....	23
6.3 CALCULATIONS FOR TANGENT MODULI.....	25
6.4 INITIAL VELOCITY OF WASTE PACKAGE.....	26
6.5 FINITE ELEMENT REPRESENTATION.....	31
7. RESULTS AND CONCLUSIONS.....	36
7.1 MESH VERIFICATION.....	36
7.2 CORNER DROP ANALYSIS .....	40
7.3 TIP-OVER FROM ELEVATED SURFACE ANALYSIS.....	42

**TABLES**

	Page
Table 5-1. List of Electronic Files in Attachment I .....	17
Table 6-1. Tangent Moduli .....	26
Table 7-1. Mesh Verification (Corner Drop) .....	36
Table 7-2. Mesh Verification (Tip-Over from Elevated Surface).....	38
Table 7-3. Wall-Averaged Stress Intensity in the Outer Corrosion Barrier (Corner Drop).....	42
Table 7-4. Wall-Averaged Stress Intensity in the Outer Corrosion Barrier (Tip-Over from Elevated Surface).....	44

**FIGURES**

	Page
Figure 3-2. Effective Plastic Strain (Tip-Over from Elevated Surface – LA Dimensions) .....	11
Figure 6-1. Corner Drop Geometry.....	26
Figure 6-2. Tip-Over from Elevated Surface Geometry .....	28
Figure 6-3. Corner Drop Standard FER .....	32
Figure 6-4. Corner Drop Refined FER.....	33
Figure 6-5. Tip-Over from Elevated Surface Standard FER.....	34
Figure 6-6. Tip-Over from Elevated Surface Refined FER .....	35
Figure 7-1. Maximum Average Through-Wall Shear Stress in the Outer Corrosion Barrier (Corner Drop – Standard Mesh).....	37
Figure 7-2. Maximum Average Through-Wall Shear Stress in the Outer Corrosion Barrier (Corner Drop – Refined Mesh) .....	37
Figure 7-3. Maximum Average Through-Wall Shear Stress in the Outer Corrosion Barrier (Tip- Over from Elevated Surface – Standard Mesh) .....	39
Figure 7-4. Maximum Average Through-Wall Shear Stress in the Outer Corrosion Barrier (Tip- Over from Elevated Surface – Refined Mesh) .....	39
Figure 7-5. Maximum Average Through-Wall Shear Stress in the Outer Corrosion Barrier (Corner Drop – Standard Mesh – SR Dimensions).....	40
Figure 7-6. Maximum Average Through-Wall Shear Stress in the Outer Corrosion Barrier (Corner Drop – Standard Mesh – Maximum Dimensions).....	41
Figure 7-7. Maximum Average Through-Wall Shear Stress in the Outer Corrosion Barrier (Corner Drop – Standard Mesh – LA Dimensions with Maximum Weight).....	41
Figure 7-8. Maximum Average Through-Wall Shear Stress in the Outer Corrosion Barrier (Tip- Over from Elevated Surface – Standard Mesh – SR Dimensions) .....	42
Figure 7-9. Maximum Average Through-Wall Shear Stress in the Outer Corrosion Barrier (Tip-Over from Elevated Surface – Standard Mesh – Maximum Dimensions) .....	43
Figure 7-10. Maximum Average Through-Wall Shear Stress in the Outer Corrosion Barrier (Tip- Over from Elevated Surface – Standard Mesh – LA Dimensions with Maximum Weight) .	43

## 1. PURPOSE

The purpose of this calculation is to determine the sensitivity of the structural response of the Naval waste packages to varying inner cavity dimensions when subjected to a corner drop and tip-over from elevated surface. This calculation will also determine the sensitivity of the structural response of the Naval waste packages to the upper bound of the naval canister masses. The scope of this document is limited to reporting the calculation results in terms of through-wall stress intensities in the outer corrosion barrier. This calculation is intended for use in support of the preliminary design activities for the license application design of the Naval waste package. It examines the effects of small changes between the naval canister and the inner vessel, and in these dimensions, the Naval Long waste package and Naval Short waste package are similar. Therefore, only the Naval Long waste package is used in this calculation and is based on the proposed/potential designs presented by the drawings and sketches in References 2.1.10 to 2.1.17 and 2.1.20. All conclusions are valid for both the Naval Long and Naval Short waste packages.

## 2. REFERENCES

### 2.1 DESIGN INPUTS

- 2.1.1 Allegheny Ludlum. 1999. "Technical Data Blue Sheet, Stainless Steels, Chromium-Nickel-Molybdenum, Types 316 (S31600), 316L (S31603), 317 (S31700), 317L (S31703)." Pittsburgh, Pennsylvania: Allegheny Ludlum Corporation. Accessed July 31, 2000. TIC: 248631. URL: [http://www.alleghenytechnologies.com/ludlum/pages/products/t316\\_317.pdf](http://www.alleghenytechnologies.com/ludlum/pages/products/t316_317.pdf)
- 2.1.2 ASM (American Society for Metals) 1961. *Properties and Selection of Metals*. Volume 1 of *Metals Handbook*. 8th Edition. Lyman, T., ed. Pages 506-507. Metals Park, Ohio: American Society for Metals. TIC: 252319.
- 2.1.3 ASM (American Society for Metals) 1980. *Properties and Selection: Stainless Steels, Tool Materials and Special-Purpose Metals*. Volume 3 of *Metals Handbook*. 9th Edition. Benjamin, D., ed. Metals Park, Ohio: American Society for Metals. TIC: 209801.
- 2.1.4 ASM International 1990. *Properties and Selection: Irons, Steels, and High-Performance Alloys*. Volume 1 of *Metals Handbook*. 10th Edition. Materials Park, Ohio: ASM International. TIC: 245666.
- 2.1.5 ASME (American Society of Mechanical Engineers) 2001. *2001 ASME Boiler and Pressure Vessel Code (includes 2002 addenda)*. New York, New York: American Society of Mechanical Engineers. TIC: 251425.
- 2.1.6 ASTM G 1-90 (Reapproved 1999). 1999. *Standard Practice for Preparing, Cleaning, and Evaluating Corrosion Test Specimens*. West Conshohocken, Pennsylvania: American Society for Testing and Materials. TIC: 238771.
- 2.1.7 Avallone, E.A. and Baumeister, T., III, eds. 1987. *Marks' Standard Handbook for Mechanical Engineers*. 9th Edition. New York, New York: McGraw-Hill. TIC: 206891.
- 2.1.8 Boyer, H.E., ed. 2000. *Atlas of Stress-Strain Curves*. Metals Park, Ohio: ASM International. TIC: 248901.
- 2.1.9 BSC (Bechtel SAIC Company) 2002. *Waste Package Tip-Over of 5-DHLW/DOE Short*. CAL-DDC-ME-000004 REV A. Las Vegas, Nevada: Bechtel SAIC Company. ACC: MOL.20020614.0038.
- 2.1.10 BSC (Bechtel SAIC Company) 2003. *Design and Engineering, Naval Long Waste Package Configuration [Sheet 1]*. 000-MW0-DNF0-00101-000-00A. Las Vegas, Nevada: Bechtel SAIC Company. ACC: ENG.20030929.0002.

2.1.11 BSC (Bechtel SAIC Company) 2003. *Design and Engineering, Naval Long Waste Package Configuration [Sheet 2]*. 000-MW0-DNF0-00102-000-00A. Las Vegas, Nevada: Bechtel SAIC Company. ACC: ENG.20030929.0003.

2.1.12 BSC (Bechtel SAIC Company) 2003. *Design and Engineering, Naval Long Waste Package Configuration [Sheet 3]*. 000-MW0-DNF0-00103-000-00A. Las Vegas, Nevada: Bechtel SAIC Company. ACC: ENG.20030929.0004.

2.1.13 BSC (Bechtel SAIC Company) 2004. *Design and Engineering, Trunnion Collar Configuration [Sheet 1]*. 100-MW0-MGR0-00101-000-00A. Las Vegas, Nevada: Bechtel SAIC Company. ACC: ENG.20040210.0003.

2.1.14 BSC (Bechtel SAIC Company) 2004. *Design and Engineering, Trunnion Collar Configuration [Sheet 2]*. 100-MW0-MGR0-00102-000-00A. Las Vegas, Nevada: Bechtel SAIC Company. ACC: ENG.20040210.0004.

2.1.15 BSC (Bechtel SAIC Company) 2005. *Naval Long Waste Package for Mass Assessment [Sheet 2]*. 000-MWK-DN00-00102-000-00A. Las Vegas, Nevada: Bechtel SAIC Company. ACC: ENG.20050819.0007.

2.1.16 BSC (Bechtel SAIC Company) 2005. *Naval Long Waste Package for Mass Assessment [Sheet 3]*. 000-MWK-DN00-00103-000-00A. Las Vegas, Nevada: Bechtel SAIC Company. ACC: ENG.20050819.0008.

2.1.17 BSC (Bechtel SAIC Company) 2005. *Naval Long Waste Package for Mass Assessment [Sheet 4]*. 000-MWK-DN00-00104-000-00A. Las Vegas, Nevada: Bechtel SAIC Company. ACC: ENG.20050819.0009.

2.1.18 BSC (Bechtel SAIC Company) 2005. *Nuclear Safety Design Bases for License Application*. 000-30R-MGR0-00400-000-003. Las Vegas, Nevada: Bechtel SAIC Company. ACC: ENG.20050929.0005.

2.1.19 Dieter, G.E. 1976. *Mechanical Metallurgy*. 2nd Edition. Materials Science and Engineering Series. New York, New York: McGraw-Hill Book Company. TIC: 247879.

2.1.20 DOE (U.S. Department of Energy) 2006. *High-Level Radioactive Waste and U.S. Department of Energy and Naval Spent Nuclear Fuel to the Monitored Geologic Repository*. Volume 1 of *Integrated Interface Control Document*. DOE/RW-0511, Rev. 2. Washington, D.C.: U.S. Department of Energy, Office of Civilian Radioactive Waste Management. ACC: DOC.20060815.0003.

2.1.21 Halliday, D.; Resnick, R.; and Merrill, J. 1988. *Fundamentals of Physics*. 3rd Edition Extended. New York, New York: John Wiley & Sons. TIC: 234765.

2.1.22 Haynes International. 1997. Hastelloy C-22 Alloy. Kokomo, Indiana: Haynes International. TIC: 238121.

2.1.23 High Temp Metals. 2002. "17-4Ph Technical Data." Sylmar, California: High Temp Metals. Accessed March 19, 2002. TIC: 252170.  
<http://www.hightempmetals.com/hitemp17-4PHdata.htm>

2.1.24 BSC (Bechtel SAIC Company) 2005. *IED Waste Package Processes, Ground Motion Time Histories, and Testing and Materials [Sheet 1 of 1]*. 800-IED-WIS0-00501-000-00A. Las Vegas, Nevada: Bechtel SAIC Company. ACC: ENG.20050406.0004.

2.1.25 LL020603612251.015. Slow Strain Rate Test Generated Stress Corrosion Cracking Data. Submittal date: 08/27/2002.

2.1.26 Naples, E.M. 1999. Thermal, Shielding, and Structural Information on the Naval Spent Nuclear Fuel (SNF) Canister. Letter from E.M. Naples (Department of the Navy) to D.C. Haught (DOE/YMSCO), August 6, 1999, with enclosures. ACC: MOL.19991001.0133.

2.1.27 Nicholas, T. 1980. *Dynamic Tensile Testing of Structural Materials Using A Split Hopkinson Bar Apparatus*. AFWAL-TR-80-4053. Wright-Patterson Air Force Base, Ohio: Air Force Wright Aeronautical Laboratories. TIC: 249469.

2.1.28 Roark, R.J. and Young, W.C. 1975. *Formulas for Stress and Strain*. 5th Edition. New York, New York: McGraw-Hill. TIC: 240746.

## 2.2 DESIGN CONSTRAINTS

2.2.1 *LS-DYNA. V.970.3858 D MPP*. 2003. HP-UX 11.22. STN: 10300-970.3858 D MPP-00.

2.2.2 BSC (Bechtel SAIC Company) 2005. *Q-List*. 000-30R-MGR0-00500-000-003. Las Vegas, Nevada: Bechtel SAIC Company. ACC: ENG.20050929.0008.

2.2.3 DOE (U.S. Department of Energy) 2003. *Validation Test Report for LS-DYNA Version 970.3858 D MPP*. 10300-VTR-970.3858 D MPP-00. Las Vegas, Nevada: U.S. Department of Energy, Office of Repository Development. ACC: MOL.20031218.0337.

2.2.4 BSC (Bechtel SAIC Company) 2006. *Quality Management Directive*. QA-DIR-10, Rev. 0. Las Vegas, Nevada: Bechtel SAIC Company. ACC: DOC.20060906.0001.

2.2.5 EG-PRO-3DP-G04B-00037, Rev. 4. *Calculations and Analyses*. Las Vegas, Nevada: Bechtel SAIC Company. ACC: ENG.20060927.0010

2.2.6 IT-PRO-0011, Rev. 1. *Software Management*. Las Vegas, Nevada: Bechtel SAIC Company. ACC: DOC.20060929.0002

2.2.7 Mecham, D.C., ed. 2004. *Waste Package Component Design Methodology Report*. 000-30R-WIS0-00100-000-002. Las Vegas, Nevada: Bechtel SAIC Company. ACC: ENG.20040713.0003.

2.2.8 Livermore Software Technology Corporation. 2003. *LS-DYNA Keyword User's Manual*. Version 970. Livermore, California: Livermore Software Technology Corporation. TIC: 254203.

### **2.3 DESIGN OUTPUTS**

None.

### 3. ASSUMPTIONS

In the course of developing this document, the following assumptions are made regarding the waste package structural calculations.

#### 3.1 ASSUMPTIONS THAT REQUIRE VERIFICATION

- 3.1.1 The dimensions, weights and materials of the waste package used in the development of this calculation, corresponding to the drawings and sketches in References 2.1.10 to 2.1.17 and 2.1.20 are assumed to be the same as the final definitive design. The rationale for this assumption is that the design of References 2.1.10 to 2.1.17 and 2.1.20 is created for the License Application (LA). This assumption is used in Section 6 and will require verification at completion of the final definitive design.

#### 3.2 ASSUMPTIONS THAT DO NOT REQUIRE VERIFICATION

- 3.2.1 Strain-rate-dependent material properties are not published in traditional sources (e.g., the ASTM, ASME and ASM standards, codes and material property data) for ASME SB-575 [UNS N06022], ASME SA-240 [UNS S31600, with modified N & C], ASME SA-36 [UNS K02600], ASME SA-240 [UNS S31603] and ASME SA-705 [UNS17400, H900 Condition], hereinafter termed Alloy 22, 316 stainless steel (SS), A 36 carbon steel (CS), 316L SS and 17-4 PH, respectively. The material properties obtained under static loading conditions are assumed for these materials. The impact of using material properties obtained under static loading conditions is anticipated to be small. The rationale for this assumption is that results presented in this calculation do not significantly change at the peak strain rates reached in the course of the corner drop and tip-over from elevated surface (see Figure 3-1, peak effective plastic strain rate [maximum slope of the curve] =  $0.242/0.001\text{ s} = 242\text{ s}^{-1}$  and Figure 3-2, peak effective plastic strain rate =  $0.043/0.0009\text{ s} = 47.8\text{ s}^{-1}$ , respectively). The presented plots are the elements characterized by the highest average effective plastic strain at the end of the simulation. For the value of strain rate in the tip-over from elevated surface case, Reference 2.1.27 (Figures 27 and 30, pp. 42 and 45, respectively) indicates only a moderate strengthening of the materials. For the value of strain rate in the corner drop case, a dramatic increase in strain occurs. This is caused by a stress riser from the discontinuity between the trunnion sleeve upper weld and outer corrosion barrier. The resulting  $242\text{ s}^{-1}$  strain rate may have a result on the strength of materials as seen in Reference 2.1.27 (Figures 27 and 30, pp. 42 and 45, respectively). However, this strain rate is present in each run and since the objective of this calculation is to compare results of dimensional and mass variability and not determine failure, any strengthening of materials will not affect the overall conclusions of this calculation. Therefore this assumption does not require verification. This assumption is used in Section 6.2 and corresponds to paragraph 5.2.5 in Reference 2.2.7.

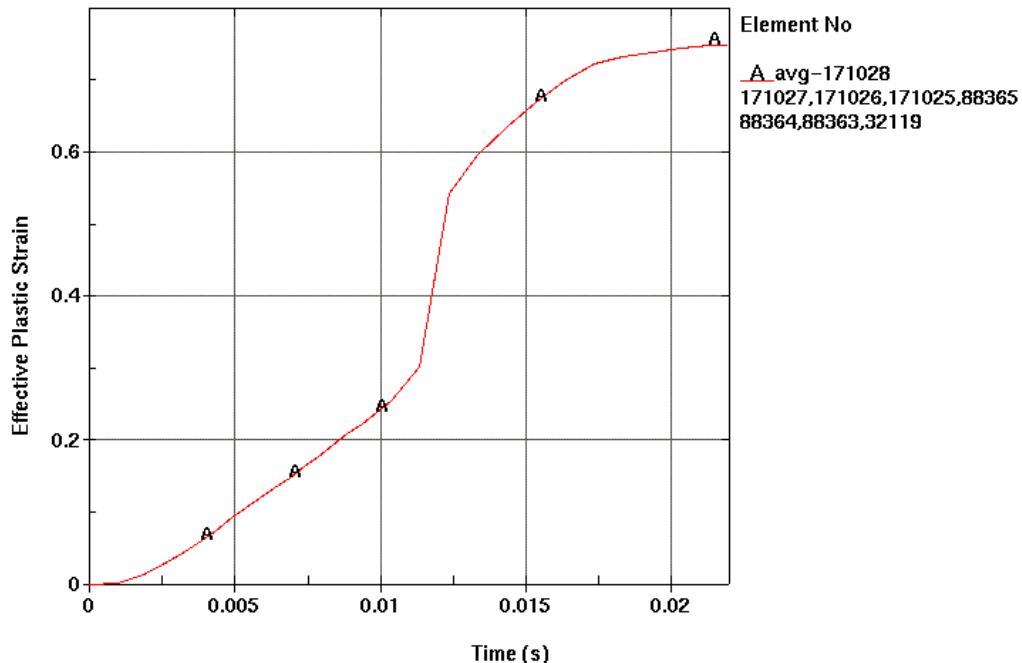


Figure 3-1. Effective Plastic Strain (Corner Drop - LA Dimensions)

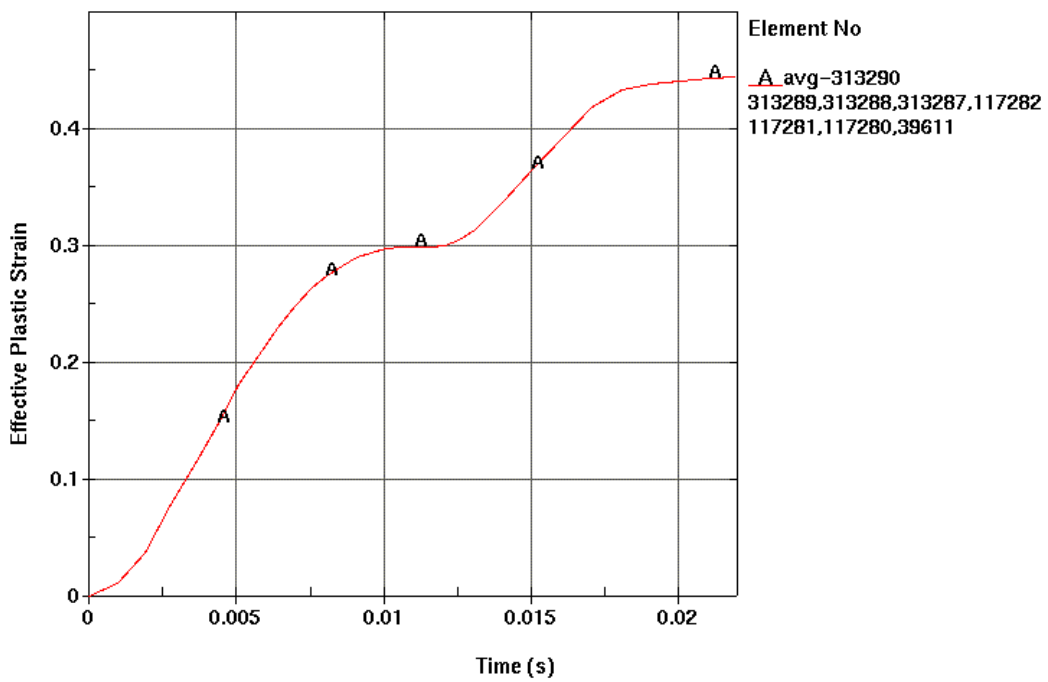


Figure 3-2. Effective Plastic Strain (Tip-Over from Elevated Surface – LA Dimensions)

3.2.2 The Poisson's ratio of Alloy 22 is not available in traditional sources. Therefore, the Poisson's ratio of ASME SB-443 [UNS N06625], hereinafter termed Alloy 625, is assumed for Alloy 22. The chemical compositions of Alloy 22 and Alloy 625 are similar since they are both 600 Series nickel-base alloys (Reference 2.1.5, Section II, Part B, SB-575, Table 1 and Reference 2.1.3, p. 143, respectively). Therefore, the difference in their Poisson's ratio is expected to be small. The rationale for this expectation is that Reference 2.1.3 pages 141, 143 and 145 indicate small differences in room temperature (RT) (20 °C) Poisson ratio values for the 600 Series nickel-base alloy family:

$$\begin{aligned}\text{Alloy 600 [UNS N06600]} &= 0.290 \\ \text{Alloy 625 [UNS N06625]} &= 0.278 \\ \text{Alloy 690 [UNS N06690]} &= 0.289\end{aligned}$$

The impact on stress results of small differences in Poisson's ratio is anticipated to be negligible. The rational for this anticipation is that the Reference 2.1.28 Table 30 stress formulas for cylindrical shells indicate insensitivity to Poisson's ratio. For the loading case of uniform radial shear loads (Case 8), the key breaching stress, the maximum hoop circumferential membrane stress, is proportional to Poisson's ratio,  $\nu$ , through the term  $(1-\nu^2)^{1/4}$ . Using the lowest and highest values of the three 600 Series nickel-base alloys'  $\nu$  values, 0.278 and 0.290, the difference in maximum hoop circumferential membrane stress values, all things being equal except  $\nu$ , is a negligible 0.2%. Therefore, this study of parametric variations provides verification of this assumption per Reference 2.2.5 page 4 ("Verification may include . . . studies of parametric variations") and further verification of this assumption is not required. This assumption is used in Section 6.2 and follows the guidance provided in paragraph 5.2.8.2 of Reference 2.2.7.

3.2.3 The RT uniform engineering strain (strain corresponding to engineering tensile strength) of Alloy 22 and 316 SS is not listed in traditional sources. Therefore, it is assumed that the RT uniform engineering strain is 90% of the RT minimum specified elongation for both materials. The rationale for this assumption is based on measurements of RT engineering stress-strain curves for the materials (Reference 2.1.8, page 304 and Reference 2.1.25, S02234\_001 Mechanical Deformation, file: "LL020603612251.015 Instron Data yr 2002"). The use of Reference 2.1.25 was approved as the appropriate data for the intended use in an Information Exchange Document (Reference 2.1.28). Therefore this assumption does not require verification. This assumption is used in Section 6.2.2 and corresponds to paragraph 5.2.6.3 of Reference 2.2.7.

3.2.4 The RT uniform engineering strain of 316L SS is not listed in traditional sources. Therefore, it is assumed that the RT uniform engineering strain is 60 percent of the RT minimum specified elongation. The rationale for this assumption is based on measurements of engineering stress-strain curves for "as-received" 316L material at moderate strain rate ( $8 \text{ s}^{-1}$ ) (Reference 2.1.8, page 305). Therefore this assumption does not require verification. This assumption is used in Section 6.2.2 and corresponds to Section 5.2.6.2 of Reference 2.2.7.

3.2.5 The RT Poisson's ratio of 316L SS is not published in traditional sources. Therefore, the RT Poisson's ratio of 316 SS is assumed for 316L SS. The chemical compositions of 316L SS and 316 SS are similar (Reference 2.1.5, Section II, Part A, SA-240, Table1) because they are both 300 Series (austenitic) stainless steels. Therefore, the difference in their Poisson's ratio is expected to be small. The rationale for this expectation is that Reference 2.1.3 page 755 Figure 15 indicates small differences in RT Poisson ratio values for the 300 Series SS family:

$$\begin{aligned}\text{Type 304 SS [UNS S30400]} &= 0.290 \\ \text{Type 316 SS [UNS S31600]} &= 0.298 \\ \text{Type 310 SS [UNS S31000]} &= 0.308\end{aligned}$$

The impact on stress results of small differences in Poisson's ratio is anticipated to be negligible. The rational for this anticipation is that the Reference 2.1.28 Table 30 stress formulas for cylindrical shells indicate insensitivity to Poisson's ratio. For the loading case of uniform radial shear loads (Case 8), the key breaching stress, the maximum hoop circumferential membrane stress, is proportional to Poisson's ratio,  $\nu$ , through the term  $(1-\nu^2)^{1/4}$ . Using the lowest and highest values of the three 300 Series stainless steels'  $\nu$  values, 0.290 and 0.308, the difference in maximum hoop circumferential membrane stress values, all things being equal except  $\nu$ , is a negligible 0.3%. Therefore, this study of parametric variations provides verification of this assumption per Reference 2.2.5 page 4 ("Verification may include . . . studies of parametric variations") and further verification of this assumption is not required. This assumption is used in Section 6.2 and is consistent with Section 5.2.8.2 of Reference 2.2.7.

3.2.6 The friction coefficients for contacts occurring between the materials used in this calculation are not published in traditional sources. It is, therefore, assumed that the dynamic (sliding) friction coefficient is 0.4 for all contacts. The rationale for this assumption is that this friction coefficient represents a reasonable lower bound value for most metal-on-metal contacts (see Reference 2.1.7, Table 3.2.1, p. 3-26). Therefore this assumption does not require verification. This assumption is used in Section 6.5 and corresponds to paragraph 5.2.14.1 of Reference 2.2.7.

3.2.7 It is assumed that the engineering stress and engineering strain are representative of the true stress and true strain for 17-4 PH. The rationale for this assumption is that the elongation equals 10% (Reference 2.1.5, Section II, Part A, SA-705/SA-705M, Table 3), and the yield strength is very close to the tensile strength, thus the difference between the engineering and true stress/strain is negligible. Therefore this assumption does not require verification. This assumption is used in Section 6.2.2.

3.2.8 The exact mass of the naval canister and contents is simplified for the purpose of this calculation in such a way that its bounding maximum weight, 44,500 kg (Reference 2.1.20, Figure C-17, Note 3), is assumed to be distributed within a solid cylinder with uniform adjusted density and constructed of unmodified SA-240 316L SS with a weight of 2 metric tons added to an interior node such that the overall center of gravity of the total mass is

located between 103 and 123 *in.* from the bottom external surface of the canister (see Reference 2.1.26, Enclosure 3, p. 3). Reference 2.1.20, Figure C-17 Note 3 also indicates that the minimum design load needs to include instrumentation error and margin, and specifies a weight increase of 4.82 metric tons above the bounding weight. An additional “maximum weight” FER was developed by adding 5 metric tons to the interior node. Although Reference 2.1.26, Enclosure 3B indicates that material with modified mechanical properties is used for the canister, nominal mechanical properties are used. The rationale for this assumption is that the same naval canister FER is used in each run and since the objective of this calculation is to compare results of dimensional and mass variability and not determine failure, a model simplification and/or variation in the material mechanical properties used will not affect the overall conclusions of this calculation. This assumption is used in Section 6.2 and 6.5.

3.2.9 The target surface is the top surface of a 0.9 *m.* length x 0.6 *m.* width x 0.5 *m.* depth base-anchored block (see Figures 6-3 through 6-6) that is assumed to be unyielding (i.e., elastic), and A 36 CS is used to represent the block in the FER. The rationale for this assumption is that lack of inelastic (energy dissipating) distortion of the target surface maximizes the stresses in the falling waste package and is therefore bounding. This assumption is used in Section 6.2 and 6.5 and corresponds to paragraph 5.2.8.1 of Reference 2.2.7.

3.2.10 The variation of functional friction coefficient between the static and dynamic value as a function of relative velocity of the surfaces in contact (see Reference 2.2.8, p. 6.9) is not published in traditional sources for the materials used in this calculation. Therefore, the effect of relative velocity of the surfaces in contact is not included in this calculation by assuming that the functional friction coefficient and static friction coefficient are both equal to the dynamic friction coefficient. The impact of this assumption on results presented in this document is anticipated to be negligible. The rationale for this assumption is that it provides a bounding set of results by minimizing the friction coefficient within the given finite element analysis framework. This assumption is used in Section 6.5 and corresponds to paragraph 5.2.14.2 of Reference 2.2.7.

3.2.11 The Poisson’s ratio and density at elevated temperatures are not published in traditional sources for Alloy 22, 316 SS, 316L SS, and 17-4 PH. The RT Poisson’s ratio and density are assumed for these materials. The impact of using RT Poisson’s ratio and density is anticipated to be small. The rationale for this assumption is that temperature sensitivities of these material properties are expected to be small and small variations will have negligible affect on the calculation’s stress results. Assumptions 3.2.2 and 3.2.5 provide parametric studies in this calculation that verify this for Poisson’s Ratio. The change in density will be downward as the material expands, inversely related to the volumetric expansion term  $(1+\Delta T\alpha)^3$ , where  $\Delta T$  is the temperature increase above RT and  $\alpha$  is the relative (to RT) coefficient of thermal expansion. Using  $\Delta T = 280^\circ\text{C}$  and a clearly upper bound value of  $10^{-6}(\text{ }^\circ\text{C})^{-1}$  for the materials’  $\alpha$  values from  $20^\circ\text{C}$  to  $300^\circ\text{C}$ , leads to a density change of less than 0.1 %. The total mass will remain unchanged, so the effect of density change on stress is unclear, however even in the unlikely event that the resulting stress effect is a magnitude

greater than the density change, it will be negligible. These studies of variations in Poisson's ratio and density provides verification of this assumption per Reference 2.2.5 page 4 ("Verification may include . . . studies of parametric variations"). Further verification of this assumption is not required. This assumption is used in Section 6.2 and is consistent with Section 5.2.8.6 of Reference 2.2.7.

3.2.12 The change of minimum elongation with increase of temperature for Alloy 22 and 316 SS is not published in traditional sources. Therefore, the magnitude of this change at  $T=300\text{ }^{\circ}\text{C}$  for Alloy 22 and 316 SS is assumed to be +10% and -30%, respectively, based on the relative change of typical elongation for said materials available in vendor catalogues (see Reference 2.1.22, p. 15, "Average Tensile Data, Solution Heat-Treated" and Reference 2.1.1, p. 8). The relative change of typical elongation should be reasonably representative of the relative change of minimum elongation. The rationale for this assumption is that the same minimum elongation is used in each run and since the objective of this calculation is to compare results of dimensional and mass variability and not determine failure, a variation in the minimum elongation used will not affect the overall conclusions of this calculation. Therefore this assumption does not require verification. This assumption is used in Section 6.2.1 and corresponds to paragraph 5.2.8.7 of Reference 2.2.7.

3.2.13 The minimum elongation of 316L SS and 17-4 PH at elevated temperatures is not available from traditional sources. These materials are not part of the outer corrosion barrier and therefore the stress in these material components are not reported in this calculation. For the purpose of this calculation, the RT elongation is assumed for these materials. The rationale for this assumption is that the same minimum elongation is used in each run and since the objective of this calculation is to compare results of dimensional and mass variability and not determine failure, a variation in the minimum elongation used will not affect the overall conclusions of this calculation. Therefore this assumption does not require verification. This assumption is used in Section 6.2.1 and 6.2.2.

## 4. METHODOLOGY

### 4.1 QUALITY ASSURANCE

This calculation is associated with the waste package design and is performed by the Thermal/Structural Analysis Group in accordance with EG-PRO-3DP-G04B-00037, *Calculations and Analyses* (Reference 2.2.5). The Naval waste package is classified as a Safety Category item (Reference 2.2.2, Table A-1, p. A-9). Therefore, this document is subject to the requirements of the *Quality Management Directive* (Reference 2.2.4, Sections 2.1.C.1.1.a.i and 17.E) and the approved version is designated as QA:QA.

### 4.2 USE OF SOFTWARE

The finite element calculation is performed by using the commercially available LS-DYNA Version (V) 970.3858 D MPP (Reference 2.2.1) finite element code, hereafter referred to as LS-DYNA.

### 4.3 STRESS ANALYSIS APPROACH

FERs of the WP with dimensional and weight differences are created and solved for drop events using LS-DYNA. The OCB stress results are reviewed to determine the maximum response locations and magnitudes. The results of this calculation are evaluated for wall-averaged stress intensities. The governing OCB stress responses for the different FERs are compared to each other to determine the sensitivity of the calculations to variations in the input parameters.

The information regarding the waste package used in this calculation is based on the proposed/potential designs presented by the drawings and sketches of References 2.1.10 to 2.1.17 and 2.1.20 (see Assumption 3.1.1). The dimensions used in this calculation refer to the dimensions associated with design for LA (Instance #5, Reference 2.1.15), Site Recommendation (SR) (Instance #15, Reference 2.1.15), and the maximum dimensions (Instance #20, Reference 2.1.15). The bounding and maximum weights used for the loaded Naval canister are provided in Reference 2.1.20.

## 5. ATTACHMENTS

Attachment I (Compact Discs 3 total): TrueGrid V2.2 and LS-DYNA V970 electronic files

Table 5-1 provides a list of attachments submitted in the form of electronic files (compact disc) in Attachment I.

Table 5-1. List of Electronic Files in Attachment I

Name	Date	Time	Size
<b>Disk 1</b>			
<b>Folder – Maxdim_corner</b>			
d3hsp	10/20/2005	4:51 pm	16,594 KB
mpp_queue	10/20/2005	4:51 pm	2 KB
naval_max.inc	10/20/2005	4:51 pm	91,045 KB
naval_max.k	10/20/2005	4:51 pm	7 KB
naval_max.tg	10/21/2005	8:11 am	384 KB
<b>Folder – nouy_corner</b>			
d3hsp	10/20/2005	4:46 pm	16,349 KB
mpp_queue	10/20/2005	4:46 pm	2 KB
naval_LA_nouy.inc	10/20/2005	4:46 pm	98,881 KB
naval_LA_nouy.tg	10/21/2005	8:10 am	384 KB
naval_nouy.k	10/20/2005	4:46 pm	7 KB
<b>Folder – refined_LAcorner</b>			
d3hsp	10/20/2005	4:50 pm	10,851 KB
mpp_queue	10/20/2005	4:50 pm	2 KB
naval_LA.k	10/20/2005	4:50 pm	7 KB
naval_LA_ref.inc	10/20/2005	4:50 pm	178,878 KB
naval_LA_ref.tg	10/21/2005	8:10 am	384 KB
<b>Folder – SR_corner</b>			
d3hsp	10/20/2005	4:50 pm	9,626 KB
mpp_queue	10/20/2005	4:50 pm	2 KB
naval_SR.inc	10/20/2005	4:50 pm	91,040 KB
naval_SR.k	10/20/2005	4:50 pm	7 KB
naval_SR.tg	10/21/2005	8:11 am	384 KB
<b>Folder – standard_LAcorner</b>			
d3hsp	10/20/2005	4:47 pm	12,568 KB
mpp_queue	10/20/2005	4:47 pm	2 KB
naval_LA.inc	10/20/2005	4:47 pm	91,035 KB
naval_LA.k	10/20/2005	4:47 pm	7 KB
naval_LA.tg	10/21/2005	8:10 am	384 KB
<b>Disk 2</b>			
<b>Folder – Maxmass_corner</b>			
d3hsp	10/20/2005	4:49 pm	16,589 KB
mpp_queue	10/20/2005	4:48 pm	2 KB
naval_LA.inc	10/20/2005	4:48 pm	91,035 KB
naval_LA.k	10/20/2005	4:48 pm	7 KB
naval_LA.tg	10/21/2005	8:12 am	384 KB
<b>Folder – nouy_tipover</b>			
d3hsp	10/20/2005	4:53 pm	31,510 KB
mpp_queue	10/20/2005	4:53 pm	2 KB
naval_LA_tipo_nouy.tg	10/21/2005	8:13 am	385 KB
naval_nouy.k	10/20/2005	4:53 pm	7 KB
naval_to_nouy.inc	10/20/2005	4:53 pm	101,237 KB

<b>Folder – SR_tipover</b>			
d3hsp	10/21/2005	8:07 am	13,657 KB
mpp_queue	10/21/2005	8:07 am	2 KB
naval_SR_tipo.k	10/21/2005	8:07 am	7 KB
naval_SR_tipo.tg	10/21/2005	8:14 am	386 KB
naval_to_SR.inc	10/21/2005	8:07 am	125,621 KB
<b>Folder – standard_LAtipover</b>			
d3hsp	10/20/2005	4:54 pm	13,655 KB
mpp_queue	10/20/2005	4:54 pm	2 KB
naval_LA_tipo.k	10/20/2005	4:54 pm	7 KB
naval_LA_tipo.tg	10/21/2005	8:13 am	386 KB
naval_to_LA.inc	10/20/2005	4:54 pm	125,649 KB
<b>Disk 3</b>			
<b>Folder – Maxdim_tipover</b>			
d3hsp	10/21/2005	8:08 am	13,654 KB
mpp_queue	10/21/2005	8:08 am	2 KB
naval_max_tipo.k	10/21/2005	8:08 am	7 KB
naval_max_tipo.tg	10/21/2005	8:14 am	386 KB
naval_to_max.inc	10/21/2005	8:08 am	125,653 KB
<b>Folder – Maxmass_tipover</b>			
d3hsp	10/21/2005	8:08 am	13,655 KB
mpp_queue	10/21/2005	8:08 am	2 KB
naval_LA_tipo.k	10/21/2005	8:08 am	7 KB
naval_LA_tipo.tg	10/21/2005	8:14 am	386 KB
naval_to_LA.inc	10/21/2005	8:08 am	125,649 KB
<b>Folder – refined_LAtipover</b>			
d3hsp	10/20/2005	4:56 pm	21,953 KB
mpp_queue	10/20/2005	4:56 pm	2 KB
naval_LA_tipo_ref.k	10/20/2005	4:56 pm	7 KB
naval_LA_tipo_ref.tg	10/21/2005	8:13 am	386 KB
naval_to_LA_ref.inc	10/20/2005	4:56 pm	255,133 KB

NOTE: The file sizes and times may vary with operating system.

## 6. CALCULATION

### 6.1 USE OF COMPUTER SOFTWARE

The qualified finite element analysis computer code used for this calculation is Livermore Software Technology Corporation LS-DYNA V970.3858 D MPP-00 (Reference 2.2.1) and is used to analyze stresses in the waste package. LS-DYNA V970 is obtained from Software Configuration Management in accordance with the appropriate procedure (Reference 2.26). LS-DYNA V970 D MPP-00 is identified by the Software Tracking Number 10300-970.3858 D MPP-00. LS-DYNA V970 is appropriate for this calculation. Test problems with known solutions were successfully performed to validate the LS-DYNA V970 application (Reference 2.2.3, Section 4 and 5). The LS-DYNA V970 evaluation performed for this calculation is fully within the range of this validation. The calculations using the LS-DYNA V970 software are executed on the Hewlett-Packard Itanium2 (IA64) series UNIX workstations (Operating System HP-UX 11.22), identified with Yucca Mountain Project tag number 501711, located in Las Vegas, Nevada. Access to the code is granted by the Software Configuration Management in accordance with the appropriate procedures.

TrueGrid V2.2 is used in this calculation solely to mesh geometric representations of the waste package in the simulations. The suitability and adequacy of this mesh is based on visual examination, engineering judgment, and the results of mesh verification in Section 7. The mesh has been evaluated in accordance with EG-PRO-3DP-G04B-00037 (Reference 2.2.5), and determined to be suitable and adequate for use as input to LS-DYNA. Therefore, the use of TrueGrid V2.2 is exempt from the requirements of IT-PRO-0011, *Software Management* (Reference 2.2.6), as defined in Section 2.1.2 of this procedure.

LS-PREPOST V1.0 (Livermore Software Technology Corporation) is the postprocessor used only for visual display and graphical representation of results and therefore is exempt from the requirements defined in Reference 2.2.6(Section 2.1.2). The post-processing is performed on the Hewlett-Packard Itanium2 (IA64) series UNIX workstations (Operating System HP-UX 11.22), identified with Yucca Mountain Project tag number 501711, and located in Las Vegas, Nevada.

The input files (identified by .k and .inc file extensions) and output files (“d3hsp”) for LS-DYNA are provided in Attachment I. LS-DYNA also uses the files “mpp\_queue” for submittal to the multiple processor system. These files define the number of processors to be used and the memory allocation for those processors. The input files for TrueGrid V2.2 (identified by .tg file extensions) are also provided in Attachment I.

## 6.2 MATERIAL PROPERTIES

Material properties used in these calculations are listed in this section. Some of the temperature-dependent strain-rate-dependent material properties are not available for Alloy 22, 316 SS, 316L SS, 17-4 PH, and A 36 CS. Therefore, all material properties listed below are obtained under static loading conditions and RT values for Poisson's ratio and density are used for these materials (see Assumptions 3.2.1 and 3.2.11).

The value of each material property is needed at 300 °C (572 °F). The material properties at 300 °C are obtained by linear interpolation of the corresponding material properties by using the formula:

$$p = p(T) = p_l + \left( \frac{T - T_l}{T_u - T_l} \right) \cdot (p_u - p_l)$$

Subscripts *u* and *l* denote the upper and lower bounding values of generic material property *p* at the corresponding bounding temperatures *T*.

ASME SB-575 [UNS N06022] (Alloy 22) (Outer corrosion barrier, outer corrosion barrier lids, trunnion sleeves, and inner vessel support ring):

- Density = 8690 kg/m<sup>3</sup> (0.314 lb/in<sup>3</sup>) (at RT) (Reference 2.1.5, Section II, Part B, SB-575, Section 7.1)
- Yield strength = 310 MPa (45.0 ksi) (at RT) (Reference 2.1.5, Section II, Part D, Table Y-1)
  - Yield strength = 216 MPa (31.4 ksi) (at 550 °F = 288 °C) (Reference 2.1.5, Section II, Part D, Table Y-1)
  - Yield strength = 211 MPa (30.6 ksi) (at 600 °F = 316 °C) (Reference 2.1.5, Section II, Part D, Table Y-1)
  - Yield strength = 214 MPa (at 572°F = 300°C)
- Tensile strength = 689 MPa (100 ksi) (at RT) (Reference 2.1.5, Section II, Part D, Table U)
  - Tensile strength = 641 MPa (92.9 ksi) (at 500°F = 260°C) (Reference 2.1.5, Section II, Part D, Table U)
  - Tensile strength = 628 MPa (91.1 ksi) (at 600°F = 316°C) (Reference 2.1.5, Section II, Part D, Table U)
  - Tensile strength = 632 MPa (at 572°F = 300°C)
- Elongation = 0.45 (at RT) (Reference 2.1.5, Section II, Part B, SB-575, Table 4)
- Poisson's ratio = 0.278 (at RT) (Reference 2.1.3, p. 143; see Assumption 3.2.2)
- Modulus of elasticity = 206 GPa (at RT) (Reference 2.1.22, p.14, Table "Average Dynamic Modulus of Elasticity"). This data is the best available and suitable.

Modulus of elasticity = 196 GPa (at 400°F = 204°C) (Reference 2.1.22, p.14, Table "Average Dynamic Modulus of Elasticity")

Modulus of elasticity = 190 GPa (at 600°F = 316°C) (Reference 2.1.22, p.14, Table "Average Dynamic Modulus of Elasticity")

Modulus of elasticity = 191 GPa (at 572°F = 300°C)

ASME SA-240 [UNS S31600, with modified N & C] (316 SS) (Inner vessel, inner vessel lids, spread ring, shell interface ring):

- Density = 7980 kg/m<sup>3</sup> (Reference 2.1.6, Table X1.1, p. 7)
- Yield strength = 207 MPa (30.0 ksi) (at RT) (Reference 2.1.5, Section II, Part D, Table Y-1)  
Yield strength = 138 MPa (20.0 ksi) (at 500°F = 260°C) (Reference 2.1.5, Section II, Part D, Table Y-1)  
Yield strength = 130 MPa (18.9 ksi) (at 600°F = 316°C) (Reference 2.1.5, Section II, Part D, Table Y-1)  
Yield strength = 132 MPa (at 572°F = 300°C)
- Tensile strength = 517 MPa (75.0 ksi) (at RT) (Reference 2.1.5, Section II, Part D, Table U)  
Tensile strength = 495 MPa (71.8 ksi) (at 500°F = 260°C) (Reference 2.1.5, Section II, Part D, Table U)  
Tensile strength = 495 MPa (71.8 ksi) (at 600°F = 316°C) (Reference 2.1.5, Section II, Part D, Table U)  
Tensile strength = 495 MPa (at 572°F = 300°C)
- Elongation = 0.40 (at RT) (Reference 2.1.5, Section II, Part A, SA-240, Table 2)
- Poisson's ratio = 0.30 (at RT) (Reference 2.1.3, Figure 15, p. 755)
- Modulus of elasticity = 195 GPa (28.3·10<sup>6</sup> psi) (RT) (Reference 2.1.5, Section II, Part D, Table TM-1)  
Modulus of elasticity = 178 GPa (25.8·10<sup>6</sup> psi) (500°F = 260°C) (Reference 2.1.5, Section II, Part D, Table TM-1)  
Modulus of elasticity = 174 GPa (25.3·10<sup>6</sup> psi) (600°F = 316°C) (Reference 2.1.5, Section II, Part D, Table TM-1)  
Modulus of elasticity = 175 GPa (at 572°F = 300°C)

ASME SA-240 [UNS S31603] (316L SS) (Naval canister, see Assumption 3.2.8):

- Yield strength = 172 MPa (25.0 ksi) (at RT) (Reference 2.1.5, Section II, Part D, Table Y-1)  
Yield strength = 113 MPa (16.4 ksi) (at 500 °F = 260 °C) (Reference 2.1.5, Section II, Part D, Table Y-1)

Yield strength = 108 MPa (15.6 ksi) (at 600 °F = 316 °C) (Reference 2.1.5, Section II, Part D, Table Y-1)

Yield strength = 109 MPa (at 572 °F = 300 °C)

- Tensile strength = 483 MPa (70.0 ksi) (at RT) (Reference 2.1.5, Section II, Part D, Table U)  
Tensile strength = 426 MPa (61.8 ksi) (at 500 °F = 260 °C) (Reference 2.1.5, Section II, Part D, Table U)  
Tensile strength = 425 MPa (61.7 ksi) (at 600 °F = 316 °C) (Reference 2.1.5, Section II, Part D, Table U)  
Tensile strength = 425 MPa (at 572 °F = 300 °C)
- Elongation = 0.40 (at RT) (Reference 2.1.5, Section II, Part A, SA-240, Table 2)
- Poisson's ratio = 0.3 (at RT) (Reference 2.1.3, Figure 15, p. 755, see Assumption 3.2.5)
- Modulus of elasticity = 195 GPa (28.3·10<sup>6</sup> psi) (at RT) (Reference 2.1.5, Section II, Part D, Table TM-1)  
Modulus of elasticity = 178 GPa (25.8·10<sup>6</sup> psi) (at 500 °F = 260 °C) (Reference 2.1.5, Section II, Part D, Table TM-1)  
Modulus of elasticity = 174 GPa (25.3·10<sup>6</sup> psi) (at 600 °F = 316 °C) (Reference 2.1.5, Section II, Part D, Table TM-1)  
Modulus of elasticity = 175 GPa (at 572 °F = 300 °C)

ASME SA-36 [UNS K02600] (A 36 CS) (Unyielding surface, see Assumption 3.2.9):

- Density = 7860 kg/m<sup>3</sup> (at RT) (Reference 2.1.6, Table X1.1, p. 7)
- Poisson's ratio = 0.30 (at RT) (Reference 2.1.4, p. 374)
- Modulus of elasticity = 203 GPa (29.5·10<sup>6</sup> psi) (at RT) (Reference 2.1.5, Section II, Part D, Table TM-1)

ASME SA-705 [UNS S17400, H900 Condition] (17-4 PH) (Trunnion collars):

- Density = 7800 kg/m<sup>3</sup> (at RT) (Reference 2.1.3, Table 12, p. 34)
- Yield strength = 1170 MPa (170 ksi) (at RT) (Reference 2.1.2, p. 506)  
Yield strength = 965 MPa (140 ksi) (at 572 °F = 300 °C) (Reference 2.1.2, p. 506)
- Tensile strength = 1310 MPa (190 ksi) (at RT) (Reference 2.1.2, p. 506)  
Tensile strength = 1100 MPa (160 ksi) (at 572 °F = 300 °C) (Reference 2.1.2, p. 506)

- Elongation = 0.10 (at RT) (Reference 2.1.5, Section II, Part A, SA-705/SA-705M, Table 3)
- Poisson's ratio = 0.272 (at RT) (Reference 2.1.23, Table "Physical Properties")
- Modulus of elasticity =  $197 \text{ GPa}$  ( $28.5 \cdot 10^6 \text{ psi}$ ) (at RT) (Reference 2.1.5, Section II, Part D, Table TM-1)  
 Modulus of elasticity =  $180 \text{ GPa}$  ( $26.1 \cdot 10^6 \text{ psi}$ ) (at  $500^\circ\text{F} = 260^\circ\text{C}$ ) (Reference 2.1.5, Section II, Part D, Table TM-1)  
 Modulus of elasticity =  $176 \text{ GPa}$  ( $25.5 \cdot 10^6 \text{ psi}$ ) (at  $600^\circ\text{F} = 316^\circ\text{C}$ ) (Reference 2.1.5, Section II, Part D, Table TM-1)  
 Modulus of elasticity =  $177 \text{ GPa}$  (at  $572^\circ\text{F} = 300^\circ\text{C}$ )

### 6.2.1 Calculations for Elevated-Temperature Elongations

The values for minimum elongation at elevated temperatures are not listed in traditional sources such as American Society for Testing and Materials (ASTM) Standards or American Society of Mechanical Engineers (ASME) Boiler and Pressure Vessel Code. However, the typical elongation values at elevated temperatures are available from vendor data. The vendor data are normalized to the minimum RT values from accepted codes (see Assumption 3.2.12).

For Alloy 22, the vendor data show an approximate 10% relative increase between RT and  $572^\circ\text{F}$  (Reference 2.1.22, p.15, Table "Average Tensile Data, Solution Heat-Treated"). Therefore, the elongation values for Alloy 22 at elevated temperatures will be as follows:

$$\text{Elongation} = 0.45 \cdot (1 + 0.1) = 0.49 \text{ (at } 572^\circ\text{F} = 300^\circ\text{C})$$

For 316 SS, the vendor data show an approximate 30% decrease between RT and  $572^\circ\text{F}$  (Reference 2.1.1, p. 8). Therefore, the elongation values for 316 SS at elevated temperatures will be as follows:

$$\text{Elongation} = 0.40 \cdot (1 - 0.3) = 0.28 \text{ (at } 572^\circ\text{F} = 300^\circ\text{C})$$

All other materials used in this calculation are not used to represent the inner vessel or outer corrosion barrier. Since the stresses in these other materials will not be reported, it is not necessary to perform similar calculations for the elongation of these materials (see Assumption 3.2.13).

### 6.2.2 Calculations for True Measures of Ductility

The material properties in Section 6.1 refer to engineering stress and strain definitions (see Reference 2.1.18, Chapter 9):

$$s = \frac{P}{A_0} \text{ and } e = \frac{L - L_0}{L_0}$$

where  $P$  stands for the force applied during static tensile test,  $L$  is the deformed-specimen length, and  $L_0$  and  $A_0$  are original length and cross-sectional area of specimen, respectively. It is generally accepted that the engineering stress-strain curve does not give a true indication of the deformation characteristics of a material during the plastic deformation since it is based entirely on the original dimensions of the specimen. Therefore, the LS-DYNA finite element code requires input in terms of true stress and strain definitions:

$$\sigma = \frac{P}{A} \text{ and } \varepsilon = \ln\left(\frac{L}{L_0}\right)$$

The relationships between the true stress and strain definitions and engineering stress and strain definitions can be readily derived based on constancy of volume ( $A_0 \cdot L_0 = A \cdot L$ ) and strain homogeneity during plastic deformation:

$$\sigma = s \cdot (1 + e) \text{ and } \varepsilon = \ln(1 + e)$$

These expressions are applicable only in the hardening region of stress-strain curve that is limited by the onset of necking.

The following parameters are used in the subsequent calculations:

$s_y \approx \sigma_y$  = yield strength

$s_u$  = engineering tensile strength

$\sigma_u$  = true tensile strength

$e_y \approx \varepsilon_y$  = strain corresponding to yield strength

$e_u$  = engineering strain corresponding to tensile strength (engineering uniform strain)

$\varepsilon_u$  = true strain corresponding to tensile strength (true uniform strain)

In absence of the uniform strain data in available literature, it needs to be estimated based on stress-strain curves and elongation (engineering strain corresponding to rupture of the tensile specimen). For Alloy 22 and 316 SS, the elongation, reduced by 10% is used in place of uniform strain (see Assumption 3.2.3). The elongation for 316L SS is reduced by 40% and used in the place of uniform strain (see Assumption 3.2.4).

In the case of Alloy 22 the true measures of ductility are:

$e_u = 0.9 \cdot \text{elongation} = 0.9 \cdot 0.45 = 0.41$  (at RT) and

$$e_u = 0.9 \cdot 0.49 = 0.44 \text{ (at } 572^{\circ}F = 300^{\circ}C\text{)}$$

$$\varepsilon_u = \ln(1 + e_u) = \ln(1 + 0.41) = 0.34 \text{ (at RT)}$$

$$\varepsilon_u = \ln(1 + e_u) = \ln(1 + 0.44) = 0.36 \text{ (at } 572^{\circ}F = 300^{\circ}C\text{)}$$

$$\sigma_u = s_u \cdot (1 + e_u) = 689 \cdot (1 + 0.41) = 971 \text{ MPa (at RT)}$$

$$\sigma_u = s_u \cdot (1 + e_u) = 632 \cdot (1 + 0.44) = 910 \text{ MPa (at } 572^{\circ}F = 300^{\circ}C\text{)}$$

For 316 SS:

$$e_u = 0.9 \cdot elongation = 0.9 \cdot 0.40 = 0.36 \text{ (at RT)}$$

$$e_u = 0.9 \cdot 0.28 = 0.25 \text{ (at } 572^{\circ}F = 300^{\circ}C\text{)}$$

$$\varepsilon_u = \ln(1 + e_u) = \ln(1 + 0.36) = 0.31 \text{ (at RT)}$$

$$\varepsilon_u = \ln(1 + e_u) = \ln(1 + 0.25) = 0.22 \text{ (at } 572^{\circ}F = 300^{\circ}C\text{)}$$

$$\sigma_u = s_u \cdot (1 + e_u) = 517 \cdot (1 + 0.36) = 703 \text{ MPa (at RT)}$$

$$\sigma_u = s_u \cdot (1 + e_u) = 495 \cdot (1 + 0.25) = 619 \text{ MPa (at } 572^{\circ}F = 300^{\circ}C\text{)}$$

For 316L SS:

$$e_u = 0.6 \cdot elongation = 0.6 \cdot 0.40 = 0.24 \text{ (at RT) (see Assumptions 3.2.4 and 3.2.13)}$$

$$\varepsilon_u = \ln(1 + e_u) = \ln(1 + 0.24) = 0.22 \text{ (at RT and } 300^{\circ}C\text{)}$$

$$\sigma_u = s_u \cdot (1 + e_u) = 483 \cdot (1 + 0.24) = 599 \text{ MPa (at RT)}$$

$$\sigma_u = s_u \cdot (1 + e_u) = 425 \cdot (1 + 0.24) = 527 \text{ MPa (at } 572^{\circ}F = 300^{\circ}C\text{)}$$

For 17-4 PH in the H900 condition, the engineering stress and engineering strain values are used for true stress and true strain values (Assumption 3.2.7).

### 6.3 CALCULATIONS FOR TANGENT MODULI

The results of this simulation were required to include elastic and plastic deformations for Alloy 22, 316 SS, 316L SS, and 17-4 PH. When the materials are driven into the plastic range, the slope of the stress-strain curve continuously changes. Thus, a simplification for this curve was needed to incorporate plasticity into the FER. A standard approximation commonly used in engineering is to use a straight line that connects the yield point and the ultimate tensile strength point of the material (bilinear elastoplastic representation). The parameters used in the subsequent calculations in addition to those defined in Section 6.2.2 are modulus of elasticity ( $E$ ) and tangent modulus ( $E_1$ ). The tangent (hardening) modulus represents the slope of the stress-strain curve in the plastic region.

In the case of Alloy 22, the strain corresponding to the yield strength is:

$$\varepsilon_y = \sigma_y / E = 214 \cdot 10^6 / 191 \cdot 10^9 = 1.12 \cdot 10^{-3} \text{ (at } 300^{\circ}C\text{) (see Sections 6.2 and 6.2.2)}$$

Hence, the tangent modulus is:

$$E_1 = (\sigma_u - \sigma_y) / (\varepsilon_u - \varepsilon_y) = (0.910 - 0.214) / (0.36 - 1.12 \cdot 10^{-3}) = 1.9 \text{ GPa} \text{ (at } 300^\circ\text{C) (see Sections 6.2 and 6.2.2)}$$

The values of tangent moduli used in this calculation are presented in Table 6-1.

Table 6-1. Tangent Moduli

Material	Tangent Modulus (GPa)
	300°C
Alloy 22	1.9
316 SS	2.2
316L SS	1.9
17-4 PH	1.5

#### 6.4 INITIAL VELOCITY OF WASTE PACKAGE

To reduce the computer execution time while preserving all features of the problem relevant to the structural calculation, the waste package is set in a position just before impact and given an appropriate initial velocity. The initial velocities are calculated using the LA dimensions and bounding masses. The effect the various dimensions and masses has on the initial velocity is negligible. Therefore the velocities calculated using the LA dimensions and bounding masses is used for each case.

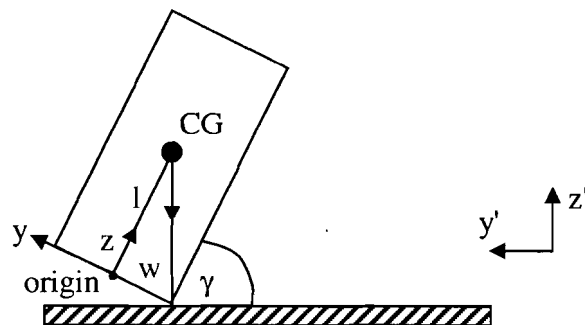


Figure 6-1. Corner Drop Geometry

Using the following parameters:

$$g = \text{acceleration due to gravity} = 9.81 \text{ m/s}^2$$

$$M = \text{total mass} = 7.15 \cdot 10^4 \text{ kg} \text{ (See References 2.1.12 and 2.1.13)}$$

LS-DYNA calculates the mass properties of the FER prior to solving the problem. The following results block was taken in the exact format from Attachment I (folder nouy\_corner, d3hsp, lines 247116 through 247143):

## principal inertias of body

```
i11 = 0.2272E+06
i22 = 0.2273E+06
i33 = 0.3592E+05
```

## summary of mass

## lumped mass in deformable

part of structure	mass
part id = 1	0.20000000E+04
part id = 2	0.72233321E+04
part id = 3	0.56971941E+03
part id = 4	0.56793854E+03
part id = 5	0.28875567E+03
part id = 6	0.00000000E+00
part id = 7	0.51454977E+02
part id = 8	0.39092509E+02
part id = 9	0.41215148E+01
part id = 10	0.44566509E+03
part id = 11	0.43166408E+01
part id = 12	0.40880638E+01
part id = 13	0.46828696E+03
part id = 14	0.44663112E+01
part id = 15	0.12134579E+05
part id = 16	0.92198556E+03
part id = 17	0.94233736E+03
part id = 18	0.30154496E+02
part id = 21	0.42986805E+05
part id = 22	0.13802790E+04

total mass = 0.71436088E+05

x-coordinate of mass center = 0.16401818E-05

y-coordinate of mass center = -0.87739086E-02

z-coordinate of mass center = 0.29403747E+01

Note: The mass from References 2.1.12 and 2.1.13 has a difference of 0.1% from that calculated by LS-DYNA V970. The effect of this difference on calculation results is negligible.

The CG was calculated using LS-DYNA with the unyielding surface omitted (see Attachment I, folder nouy\_corner, d3hsp). LS-DYNA calculates the mass properties of the FER prior to solving the problem. The CG was found to be 2.940 m in vertical (z) direction from the bottom of the waste package along the centerline.

$l = 2.940 \text{ m}$  = distance in the z direction from the origin to the CG. The origin is at the center of the waste package in the x and y direction and at the bottom edge of the waste package in the z direction (see Figure 6-1).

$w = 1.074 \text{ m}$  = outer radius of the lifting collar (see References 2.1.13 and 2.1.14)

The angle of inclination the waste package makes with the unyielding surface (see Figure 6-1) is defined as:

$$\gamma = \tan^{-1}\left(\frac{l}{w}\right) = \tan^{-1}\left(\frac{2.940}{1.074}\right) = 70^\circ$$

Using Newton's equation of motion (Reference 2.1.21, p. 20, equation 15) and a drop height of  $6.5 \text{ ft}$  ( $2.0 \text{ m}$ ) (see Reference 2.1.18, Table A-II, p. A-46):

$$\begin{aligned} V_f^2 &= V_0^2 + 2 \cdot g \cdot (h_0 - h_f) \\ V_f^2 &= 0^2 + 2 \cdot 9.81 \text{ m/s}^2 \cdot 2.0 \text{ m} \\ V_f &= 6.3 \text{ m/s} \end{aligned}$$

The drop height for the Naval Long waste package is limited to  $3.3 \text{ ft}$  ( $1 \text{ m}$ ) (see Reference 2.1.18, Table A-II, p. A-46). The simulations are performed using the higher drop height of  $2 \text{ m}$  to accentuate the comparisons.

Therefore, the initial velocity in the negative  $z'$  direction is  $6.3 \text{ m/s}$  for a  $2.0 \text{ m}$  drop height. For use in LS-DYNA with the coordinate system denoted with  $y$  and  $z$  in Figure 6-1, this velocity must be converted. Therefore in the prime coordinate system:

$$\begin{aligned} V_y &= -6.3 \text{ m/s} \cdot \cos(\gamma) = -6.3 \text{ m/s} \cdot \cos(70) = -2.2 \text{ m/s} \\ V_z &= -6.3 \text{ m/s} \cdot \sin(\gamma) = -6.3 \text{ m/s} \cdot \sin(70) = -5.9 \text{ m/s} \end{aligned}$$

For the tip-over from elevated surface, the angular velocity just before impact is calculated.

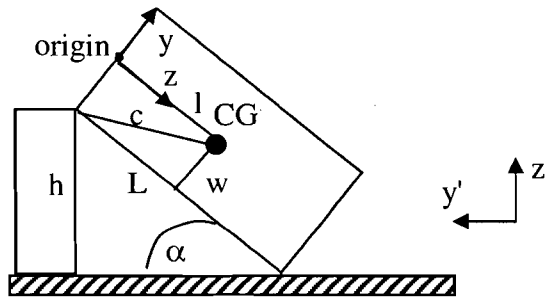


Figure 6-2. Tip-Over from Elevated Surface Geometry

$L = 5.812 \text{ m}$  = total length of the waste package (see Figure 6-2 and Reference 2.1.11).

$h = 6.5 \text{ ft}$  ( $2 \text{ m}$ ) = height of elevated surface greater than the Naval Long height of  $1.6 \text{ ft}$  ( $0.5 \text{ m}$ ) (see Reference 2.1.18, Table A-II, p. A-46). Again the simulations are performed using the higher height of  $2 \text{ m}$  to accentuate the comparisons.

The angle of inclination the waste package makes with the unyielding surface (see Figure 6-2) is defined as:

$$\alpha = \sin^{-1}\left(\frac{h}{L}\right) = \sin^{-1}\left(\frac{2}{5.812}\right) = 20^\circ$$

For the tip-over from an elevated surface, the most conservative means to calculate the highest rotational velocity is to start with the waste package just before tipping over with all the internal components in contact with the bottom of the waste package, as in the corner drop case.

Therefore in this case, the waste package is rotating about the x axis,  $I_x = I_{11} = 2.272 \cdot 10^5 \text{ kg} \cdot \text{m}^2$  (see Figure 6-1).

The starting angle the waste package needs to tip about its outer edge of the trunnion collar sleeve is the same as for the corner drop and is  $\gamma = 70^\circ$  (see Figure 6-2).

$$c = \sqrt{l^2 + w^2} = \sqrt{2.940^2 + 1.074^2} = 3.130 \text{ m}$$

Using the parallel axis theorem, the mass moment of inertia about the point of rotation:

$$I = I_x + Mc^2 = 2.272 \cdot 10^5 + 7.15 \cdot 10^4 \cdot 3.130^2 = 9.28 \cdot 10^5 \text{ kg} \cdot \text{m}^2$$

Using Newton's second law of motion:

$$\sum M = I \cdot \alpha$$

$M \cdot g \cdot c \cdot \cos \theta = I \cdot \alpha$ , where  $\theta$  is the angle of rotation and  $\alpha$  is the rotational acceleration it follows that:

$$\alpha = \frac{M \cdot g \cdot c \cdot \cos \theta}{I} = \frac{7.15 \cdot 10^4 \cdot 9.81 \cdot 3.130 \cdot \cos \theta}{9.28 \cdot 10^5} = 2.37 \cdot \cos \theta$$

Knowing:

$v = \frac{ds}{dt}$  and  $a = \frac{dv}{dt}$ , where  $s$  is displacement,  $v$  is velocity, and  $a$  is acceleration, velocity in terms of acceleration can be found by rearranging and substituting:

$$dt = \frac{dv}{a}$$

$$v = \frac{ds}{\frac{dv}{a}} = \frac{ds}{a}$$

$$v \cdot \frac{dv}{a} = ds$$

Thus:  $v \cdot dv = a \cdot ds$  or for rotational velocity:  $\omega \cdot d\omega = \alpha \cdot d\theta$

The total angle of rotation for the tip-over is therefore the starting angle  $\gamma$  plus the final angle  $\alpha$ , or  $90^\circ$ . Integrating over this angle of rotation:

$$\int_0^\omega \omega \cdot d\omega = \int_0^{\frac{\pi}{2}} \alpha \cdot d\theta$$
$$\frac{\omega^2}{2} = 2.37 \cdot (\sin \theta) \Big|_{\frac{\pi}{2}}^{\gamma} = 2.37 \cdot \left[ \sin\left(\frac{\pi}{2}\right) - \sin(0) \right] = 2.37$$
$$\omega = 2.18 \frac{\text{rad}}{\text{s}}$$

## 6.5 FINITE ELEMENT REPRESENTATION

Full three-dimensional FERs are developed in TrueGrid V2.2. The dimensions used in this calculation refer to the dimensions associated with design for LA (Instance #5, Reference 2.1.15), SR (Instance #15, Reference 2.1.15), and the maximum dimensions (Instance #20, Reference 2.1.15) using the dimensions provided in References 2.1.10 through 2.1.17 (see Assumption 3.1.1). The simplifications and (bounding and maximum) masses used for the loaded Naval canister are provided in Reference 2.1.20 and Assumption 3.2.8. Additionally, the lid lifting features are omitted. The benefit of using this approach is to reduce the computer execution time while preserving all features of the problem relevant to the structural calculation.

The target surface is conservatively assumed to be unyielding A 36 CS (Assumption 3.2.9).

The initial drop height is reduced to 0.1 *mm*, and the waste package is given an initial translational or rotational velocity corresponding to its rigid-body motion at contact (see Section 6.4).

A static and dynamic friction coefficient of 0.4 is assumed for all contacts (Assumptions 3.2.6 and 3.2.10).

The orientation of the waste package and its contents are in the worst scenario hypothesized by Section 5.6 of Reference 2.1.9. This is on the edge where the cutaway trunnion sleeve is in transition and the inner vessel and outer corrosion barrier, as well as internals are in contact prior to impact. Reference 2.1.9, Section 6, shows that this orientation creates the highest stresses in the outer corrosion barrier and inner vessel.

The standard mesh is generated using 8-node constant-stress brick elements and is refined in the regions of welds and corners where the maximum stresses occur. To capture realistic wall stresses, the outer corrosion barrier utilizes 8 brick elements across the wall thickness and is generated in each of the other directions (hoop and axial) to maintain an aspect ratio of approximately 1:1:1 in the regions of interest (see Figures 6-3 and 6-5). The mesh is then gradually transitioned away from these areas of interest to reduce the number of elements and thus reduce the computer execution time.

The termination time for most computer runs is set to 0.022 s. This termination time is sufficiently large to capture the maximum stresses.

The mesh is further refined to verify the results are not mesh sensitive in accordance with Reference 2.2.7, Section 6.2.3. The number of brick elements across the thickness of the outer corrosion barrier is increased from 8 elements to 11 elements and the number of elements in the other directions are increased to result in an aspect ratio of approximately 1:1:1 in the region of interest (see Figure 6-4 for the corner drop and Figure 6-6 for the tip-over from elevated surface). These comparative results can be seen in Tables 7-1 and 7-2. Thus, the accuracy and representativeness of the results of this calculation are acceptable.

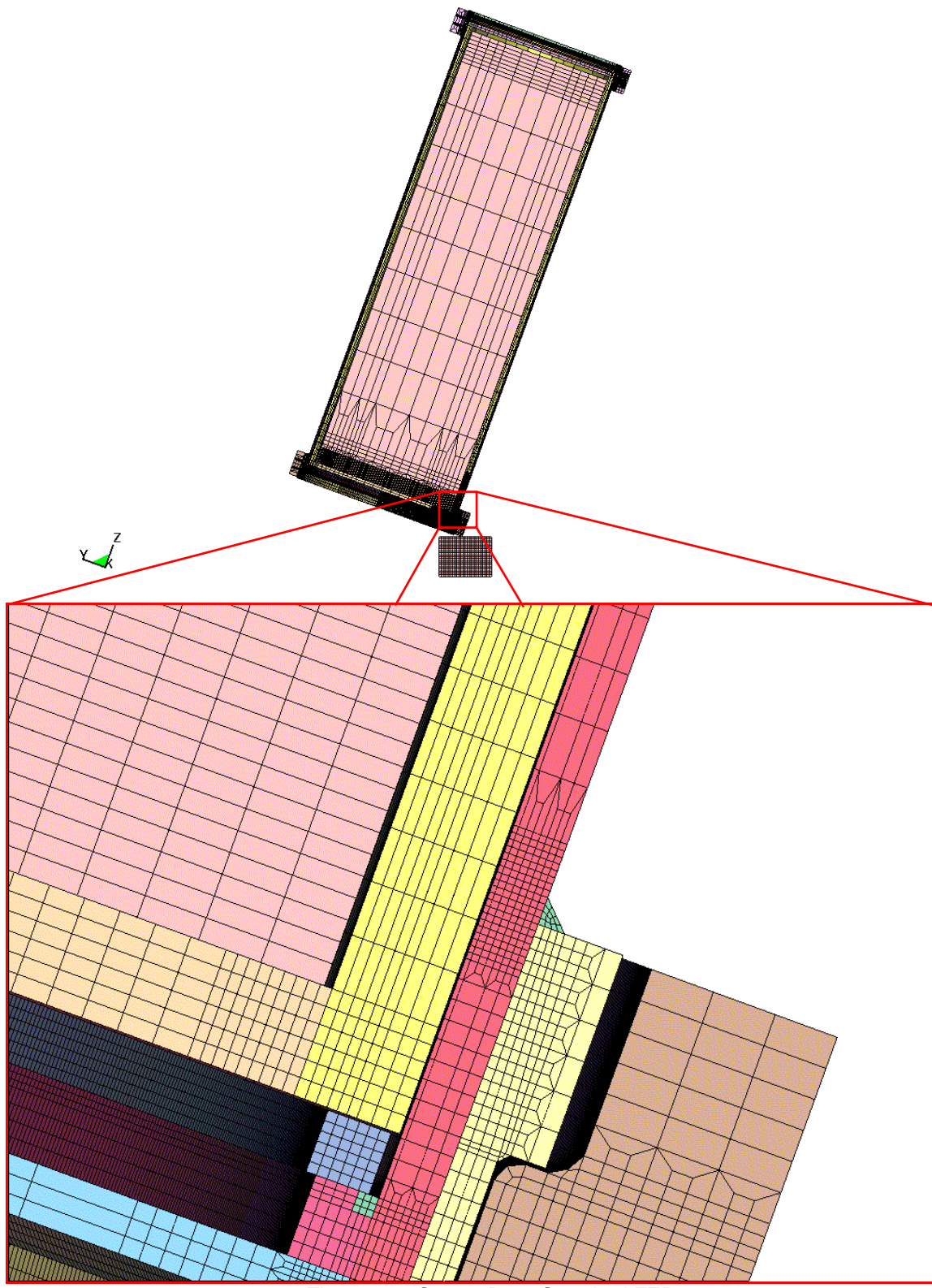


Figure 6-3. Corner Drop Standard FER

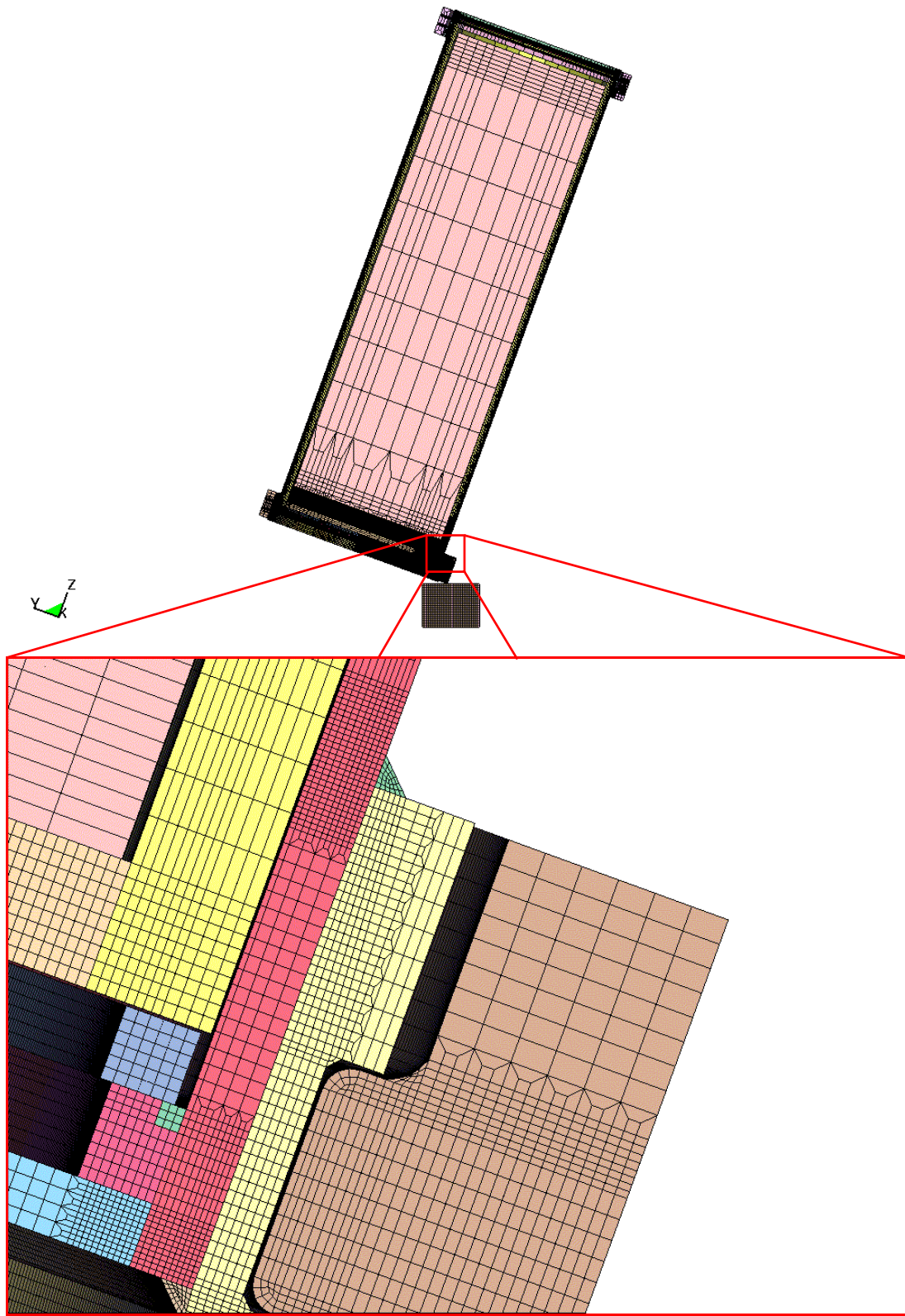


Figure 6-4. Corner Drop Refined FER

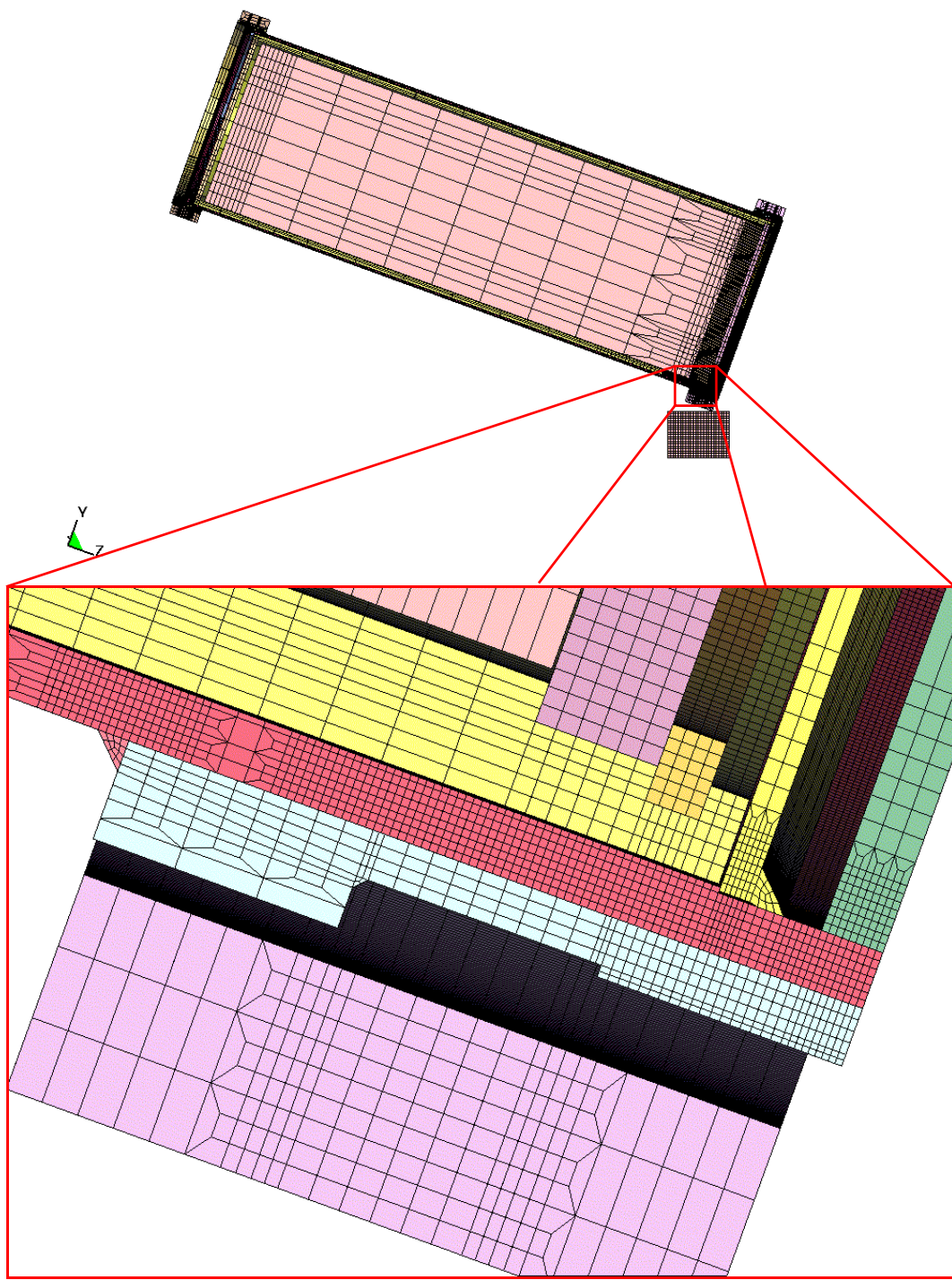


Figure 6-5. Tip-Over from Elevated Surface Standard FER

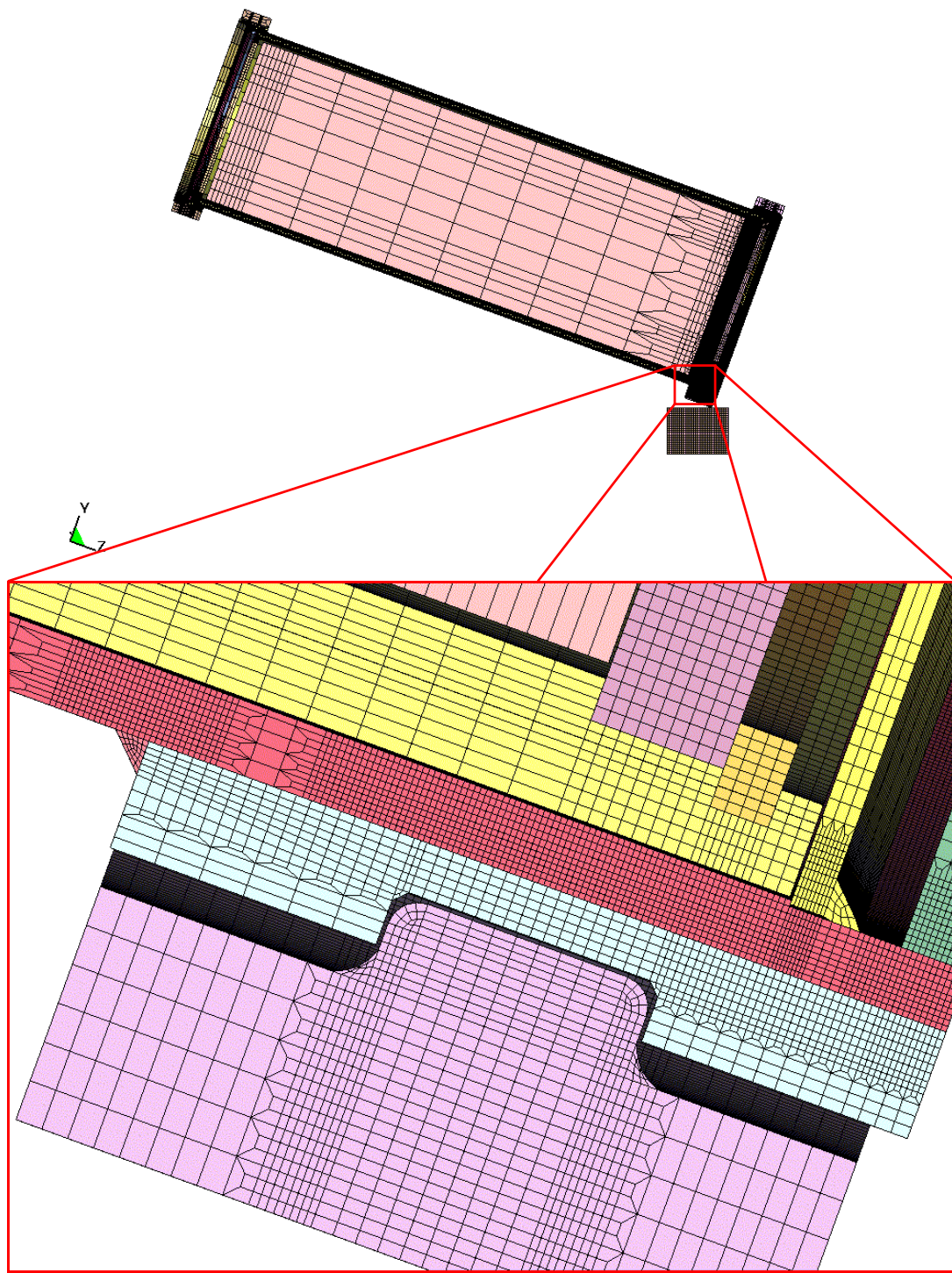


Figure 6-6. Tip-Over from Elevated Surface Refined FER

## 7. RESULTS AND CONCLUSIONS

The following results obtained from LS-DYNA are reasonable compared to the inputs and are suitable for the intended use of this calculation.

### 7.1 MESH VERIFICATION

Table 7-1 shows the changes of volumes and time-maximum average through-wall shear stresses ( $\tau_{avg}$ ) between the standard and refined mesh for the corner drop. The elements reported in Table 7-1 are the elements of the stress classification line through the outer corrosion barrier at the location with the maximum average through-wall shear stress. The initial volume (V) reported in Table 7-1 is for the outer element of the stress classification line.

Table 7-1. Mesh Verification (Corner Drop)

	<b>Element #s</b>	<b>Standard Mesh</b>	<b>Element #s</b>	<b>Refined Mesh</b>	<b>% Change</b>
Outer Corrosion Barrier	171028 171027 171026 171025 88365 88364 88363 32119	$\tau_{avg} = 5.450e+8 \text{ Pa}$ (see Figure 7-1)	341382 341381 341380 341379 341378 341377 158974 158973 158972 158971 49072	$\tau_{avg} = 5.582e+8 \text{ Pa}$ (see Figure 7-2)	2.4%
	171028	$V = 3.602e-8 \text{ m}^3$	341382	$V = 1.502e-8 \text{ m}^3$	140%

Table 7-1 shows the change in maximum average through-wall shear stress is more than an order of magnitude lower than the corresponding change in element volume. This verifies that the standard mesh is appropriate for the corner drop simulation (see Reference 2.2.7, Section 6.2.3).

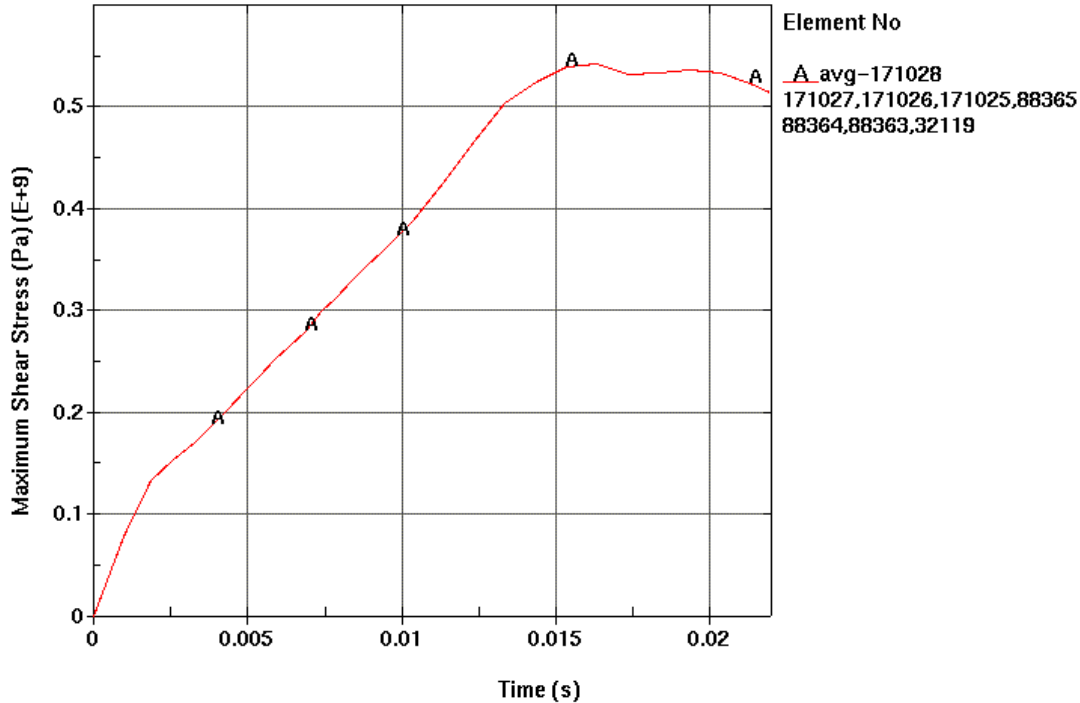


Figure 7-1. Maximum Average Through-Wall Shear Stress in the Outer Corrosion Barrier (Corner Drop – Standard Mesh)

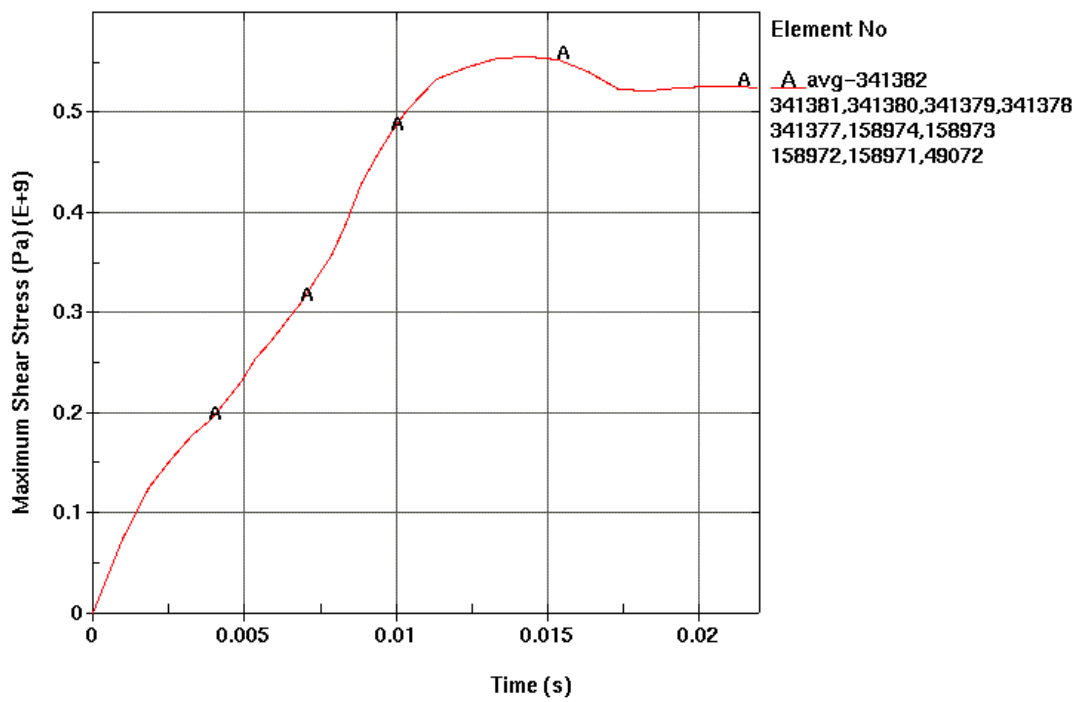


Figure 7-2. Maximum Average Through-Wall Shear Stress in the Outer Corrosion Barrier (Corner Drop – Refined Mesh)

Table 7-2 shows the changes of volumes and maximum average through-wall shear stresses between the standard and refined mesh for the tip-over from elevated surface. The elements reported in Table 7-2 are the elements of the stress classification line through the outer corrosion barrier at the location with the maximum average through-wall shear stress. The initial volume reported in Table 7-2 is for the outer element of the stress classification line.

Table 7-2. Mesh Verification (Tip-Over from Elevated Surface)

	<b>Element #s</b>	<b>Standard Mesh</b>	<b>Element #s</b>	<b>Refined Mesh</b>	<b>% Change</b>
Outer Corrosion Barrier	313290 313289 313288 313287 117282 117281 117280 39611	$\tau_{avg} = 4.247e+8 \text{ Pa}$ (see Figure 7-3)	629532 629531 629530 629529 629528 629527 209344 209343 209342 209341 61465	$\tau_{avg} = 4.247e+8 \text{ Pa}$ (see Figure 7-4)	0.0%
	313290	$V = 3.737e-8 \text{ m}^3$	629532	$V = 1.557e-8 \text{ m}^3$	140%

Table 7-2 shows the change in maximum average through-wall shear stress is more than an order of magnitude lower than the corresponding change in element volume. This verifies that the standard mesh is appropriate for the tip-over from elevated surface simulation (see Reference 2.2.7, Section 6.2.3).

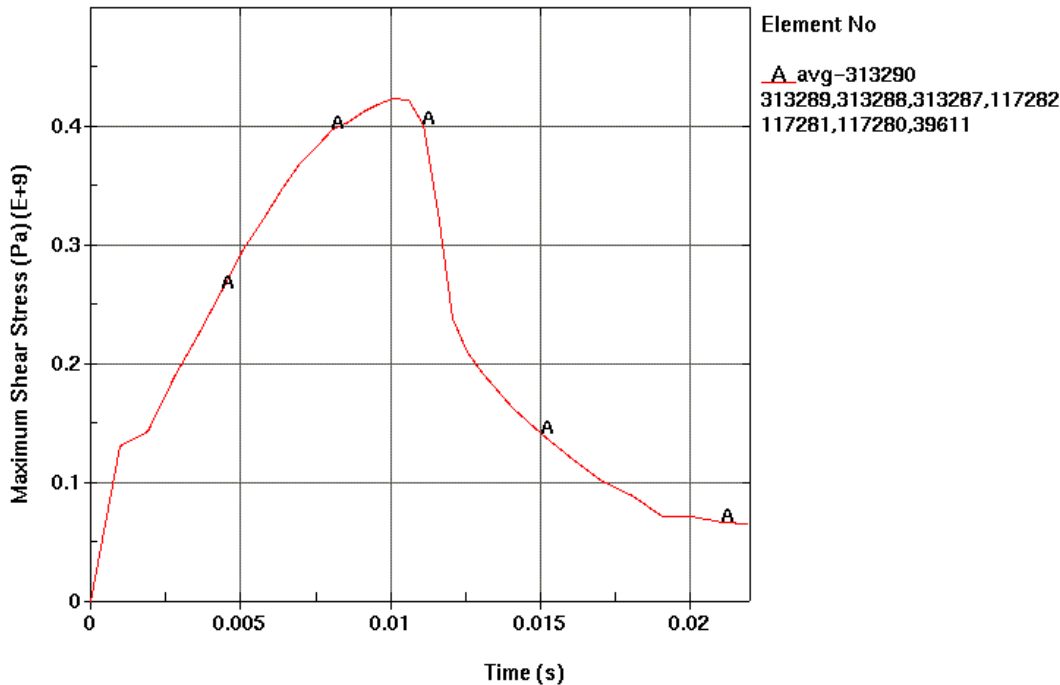


Figure 7-3. Maximum Average Through-Wall Shear Stress in the Outer Corrosion Barrier  
(Tip-Over from Elevated Surface – Standard Mesh)

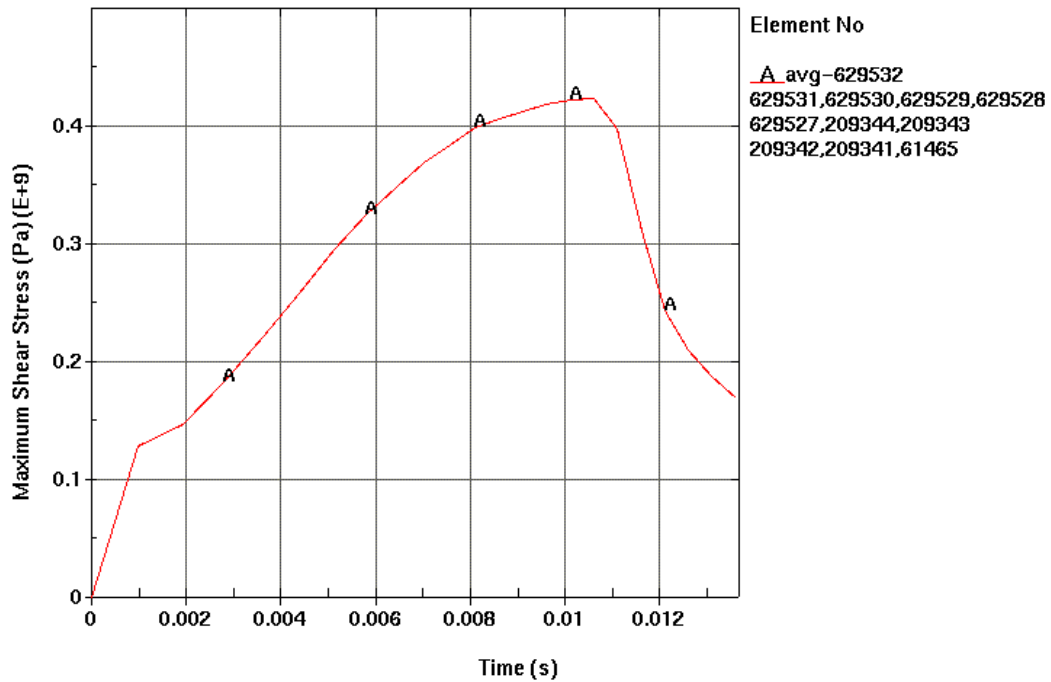


Figure 7-4. Maximum Average Through-Wall Shear Stress in the Outer Corrosion Barrier  
(Tip-Over from Elevated Surface – Refined Mesh)

The results obtained from LS-DYNA are reported in terms of maximum shear stress. Since the maximum ASME membrane stress intensities are used in design evaluations and are the basis of these comparisons, the results needed to be converted. The maximum shear stress (see Reference 2.1.18, Chapter 3) is defined as one-half of the difference between the maximum and minimum principal stress. ASME stress intensity is defined as the difference between the maximum and minimum principal stress (see Reference 2.1.5, Section III, Division 1, Appendix XIII, XIII-1123(a)). The wall-average of twice the maximum shear stress is a conservative approximation of the ASME membrane stress intensity (see Reference 2.2.7, Section 6.2.4)

The maximum ASME membrane stress intensities are found by carefully examining each reported time step taken by LS-DYNA, using LS-POST, which graphically highlights the surfaces with the highest magnitude of maximum shear stress, at each time step. These regions are interrogated by LS-POST to find the line of through-wall elements with the time-maximum of the wall-averaged maximum shear stresses.

## 7.2 CORNER DROP ANALYSIS

Figure 7-5 presents the average through-wall shear stress time history plots of the outer corrosion barrier at the location of maximum average through-wall shear stress for the corner drop using the SR dimensions. Figure 7-6 presents a corresponding plot using the maximum dimensions. Figure 7-7 presents a corresponding plot using the LA dimensions with the mass of the naval canister increased to the maximum of 49.32 metric tons (Reference 2.1.20, Figure C-17). Table 7-3 contains the wall-averaged total stress intensities and their ratios to the ultimate strengths at 300°C, as well as the percentage difference in results from the results using the LA dimensions (Figure 7-1).

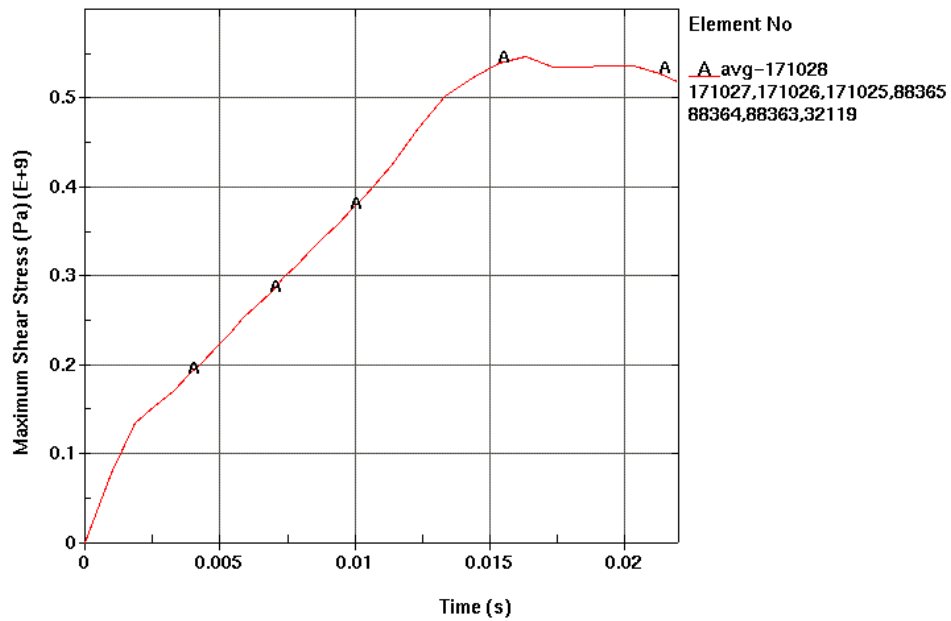


Figure 7-5. Maximum Average Through-Wall Shear Stress in the Outer Corrosion Barrier (Corner Drop – Standard Mesh – SR Dimensions)

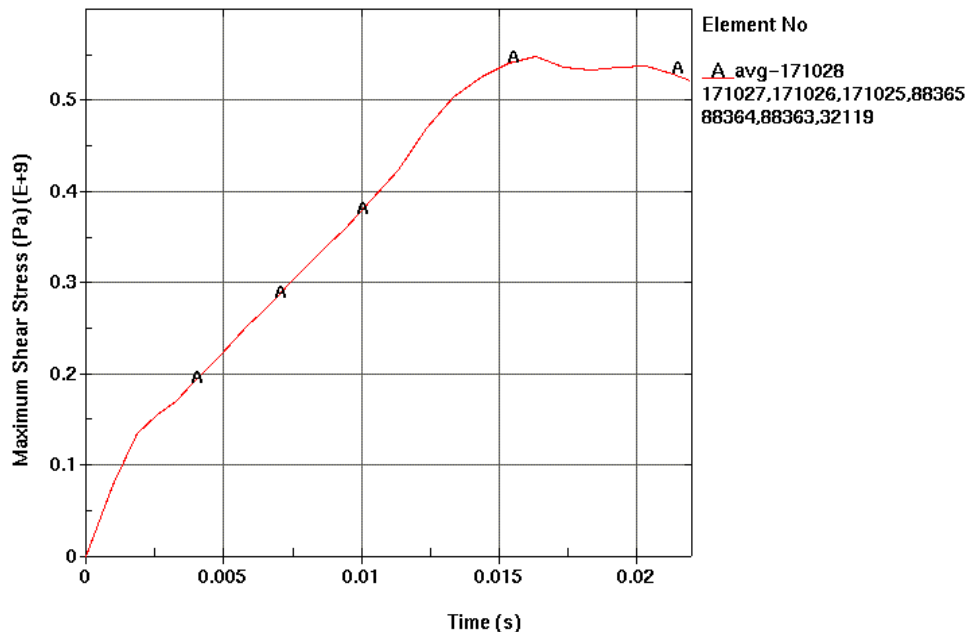


Figure 7-6. Maximum Average Through-Wall Shear Stress in the Outer Corrosion Barrier  
(Corner Drop – Standard Mesh – Maximum Dimensions)

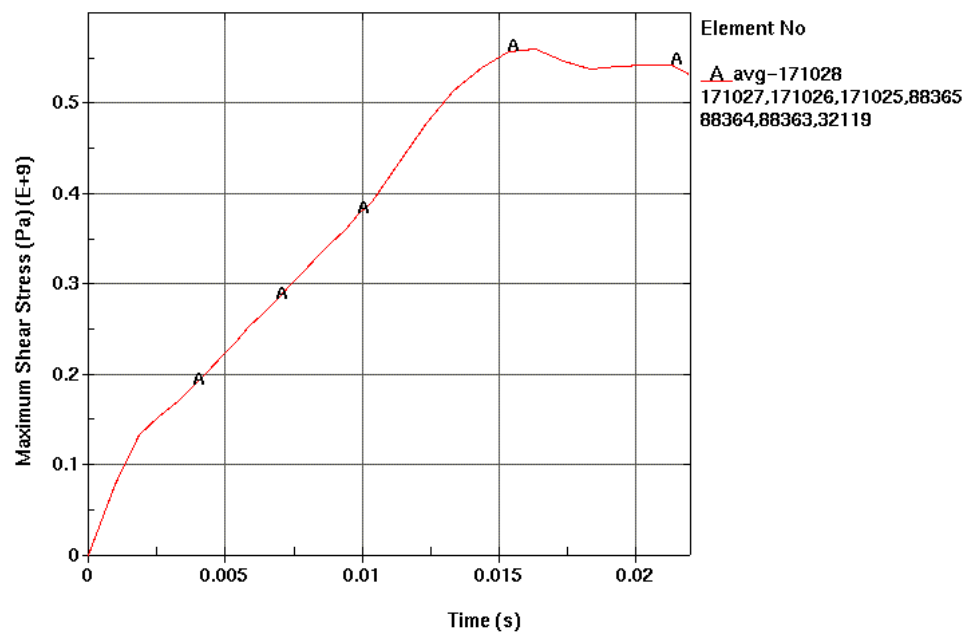


Figure 7-7. Maximum Average Through-Wall Shear Stress in the Outer Corrosion Barrier  
(Corner Drop – Standard Mesh – LA Dimensions with Maximum Weight)

Table 7-3. Wall-Averaged Stress Intensity in the Outer Corrosion Barrier (Corner Drop)

	Wall-Averaged Stress Intensity ( $P_L$ )	Difference from LA	$P_L/\sigma_u$
LA Dimensions	1090 MPa (see Figure 7-1)	-	1.20
SR Dimensions	1096 MPa (see Figure 7-5)	+0.6%	1.20
Maximum Dimensions	1100 MPa (see Figure 7-6)	+0.9%	1.21
LA Dimensions with Maximum Weight	1124 MPa (see Figure 7-7)	+3.1%	1.24

From Table 7-3, the dimensions of the waste package have essentially no affect on the stresses from the corner drop and the maximum weight of the naval canister has only a slight affect.

### 7.3 TIP-OVER FROM ELEVATED SURFACE ANALYSIS

Figure 7-8 presents the average through-wall shear stress time history plots of the outer corrosion barrier at the location of maximum average through-wall shear stress for the tip-over from elevated surface using the SR dimensions. Figure 7-9 presents a corresponding plot using the maximum dimensions. Figure 7-10 presents a corresponding plot using the LA dimensions with the mass of the naval canister increased to the maximum of 49.32 metric tons (Reference 2.1.20, Figure C-19). Table 7-4 contains the wall-averaged total stress intensities and their ratios to the ultimate strengths at 300°C, as well as the percentage difference in results from the results using the LA dimensions.

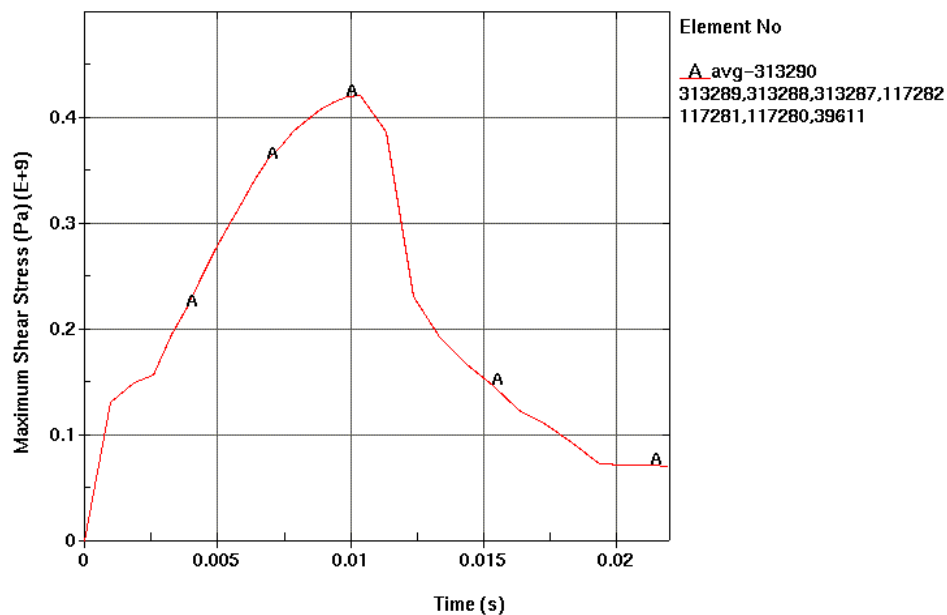


Figure 7-8. Maximum Average Through-Wall Shear Stress in the Outer Corrosion Barrier (Tip-Over from Elevated Surface – Standard Mesh – SR Dimensions)

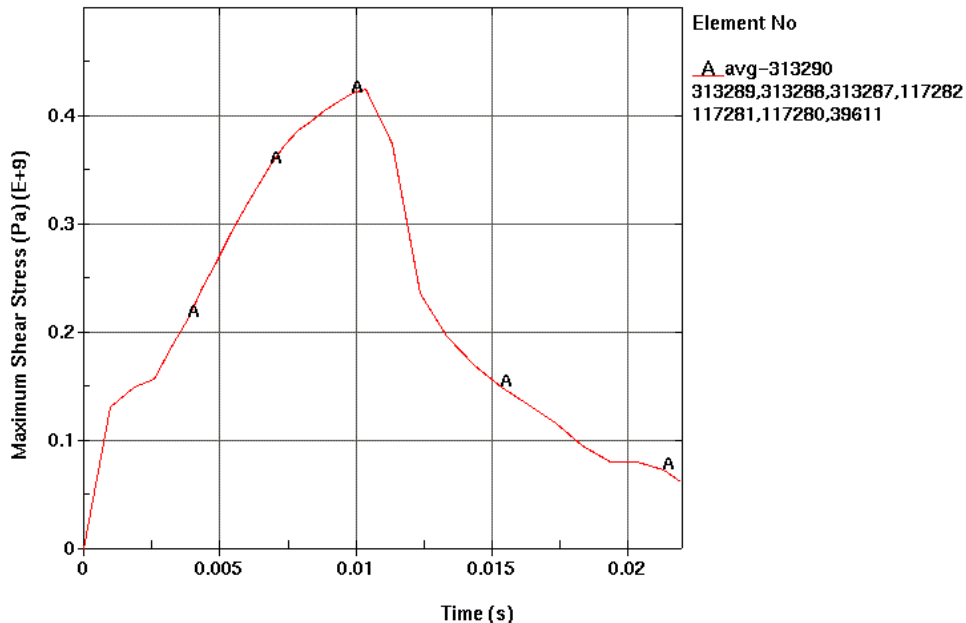


Figure 7-9. Maximum Average Through-Wall Shear Stress in the Outer Corrosion Barrier (Tip-Over from Elevated Surface – Standard Mesh – Maximum Dimensions)

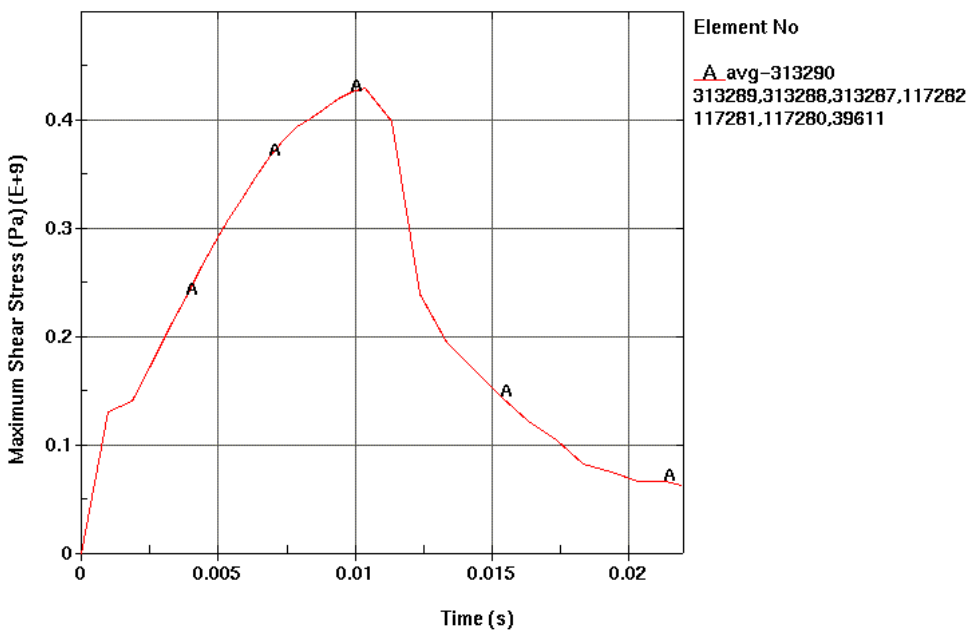


Figure 7-10. Maximum Average Through-Wall Shear Stress in the Outer Corrosion Barrier (Tip-Over from Elevated Surface – Standard Mesh – LA Dimensions with Maximum Weight)

Table 7-4. Wall-Averaged Stress Intensity in the Outer Corrosion Barrier  
(Tip-Over from Elevated Surface)

	Wall-Averaged Stress Intensity ( $P_L$ )	Difference from LA	$P_L/\sigma_u$
LA Dimensions	849 MPa (see Figure 7-3)	-	0.93
SR Dimensions	846 MPa (see Figure 7-8)	-0.4%	0.93
Maximum Dimensions	853 MPa (see Figure 7-9)	+0.5%	0.94
LA Dimensions with Maximum Weight	862 MPa (see Figure 7-10)	+1.5%	0.95

From Table 7-4, the dimensions of the waste package have essentially no effect on the stresses from the tip-over from elevated surface and the maximum weight of the naval canister has only a slight effect.